

1
2
3
4
5
6
7
8
9
10
11
12
13
14
15
16
17
18
19
20
21
22
23
24
25
26
27
28
29
30
31
32
33
34
35
36
37
38
39
40
41
42
43
44
45
46
47
48
49
50
51
52

Reviewer 1

We would like to thank Reviewer #1 for his/her review of our paper and the important comments and suggestions provided. Please, find below our responses to the Reviewer's comments and the details on how we address them in the new version of the manuscript.

1.1) Line 27: This approach has been used before so it's not accurate to call it innovative. Zhao and Weng (2002, <http://www.jstor.org/stable/26184983>) retrieved ice cloud parameters by isolating ice scattering signature. The latter is derived from observed high frequency TBs and simulated cloud base (i.e. clear-sky) TBs. They calculated the over land cloud base high frequency TBs from low frequencies with the assumption that low frequency measurements are less affected by cloud scattering. Please modify the manuscript accordingly and cite Zhao and Weng's paper.

Thanks to the reviewer for the very useful suggestion. The HANDEL-ATMS approach is indeed very similar to Zhao&Weng's approach. However, it is also worth noticing some important differences:

- 1) the Zhao&Weng Algorithm screens out all possible "scattering surfaces" including snow cover and sea ice, that are the kind of surfaces where HANDEL-ATMS is focused on.
- 2) the Simulated clear-sky TB estimated by Zhao&Wheng is obtained by an empirical relationship between AMSU-A 23 and 31 GHz and 89 and 150 GHz clear-sky TB; in our work, an emissivity spectrum has been estimated for the ATMS channels downstream a background surface classification and the differences between the observed signal and the simulated one for 16 different channels have been used as input of a neural network approach

Moreover in the Abstract we stated:

The main novelty of the approach is the radiometric characterization of the background surface (including snow covered land and sea ice) at the time of the overpass to derive multi-channel surface emissivities and clear-sky contribution to be used in the snowfall retrieval process.

The statement in parenthesis, in our opinion, is sufficient to restrict the novelty of the approach to some background surfaces. Therefore we would like to keep the abstract as it is. However, we recognize the importance of the Zhao&Weng approach and the similarities between that work and HANDEL-ATMS and we modified the Introduction (lines 99-121):

From:

The main novelty of the approach is the exploitation of the ATMS wide range of channels (from 22 GHz to 183 GHz) to obtain the radiometric characterization of the background surface at the time of the overpass. The derived surface emissivities are used to infer the clear-sky contribution to the measured TBs in the high frequency channels in the snowfall retrieval process. Moreover, the algorithm is based on the exploitation of an observational dataset where each ATMS multichannel observation is associated with coincident (in time and space) CloudSat CPR vertical snow profile and surface snowfall rate (hereafter ATMS-CPR coincidence dataset). Several snowfall retrieval algorithms for cross-track scanning radiometers have evolved in the last 20 years starting from the Advanced Microwave Sounder Unit-B (AMSU-B) (Kongoli et al, 2003, Skofronick-Jackson et al, 2004, Noh et al., 2009, Liu and Seo 2013), and Microwave Humidity Sounder (MHS) (see Liu & Seo, 2013, Edel et al, 2020), and evolving to ATMS (Kongoli et al, 2015, Meng et al, 2017, Kongoli et al, 2018, You et al, 2022, Sanò et al, 2022). Some of them are based on radiative transfer simulations of observed snowfall events (Kongoli et al, 2003, Skofronick-Jackson et al, 2004, Kim et al, 2008), or on in-situ data (see Kongoli et al, 2015, Meng et al, 2017, Kongoli et al, 2018), others on CPR observations (Edel et al, 2020, You et al, 2022, Sanò et al, 2022), or a combination of them (Noh et al, 2009, Liu & Seo, 2013).

to:

The main novelty of the approach is the exploitation of the ATMS wide range of channels (from 22 GHz to 183 GHz) to obtain the radiometric characterization of the background surface at the time of the overpass. The derived surface emissivities are used to infer the clear-sky contribution to the measured TBs in the high frequency

53 channels in the snowfall retrieval process. This approach is similar to the work of Zhao and Weng, 2002, for
54 AMSU observations limited to non-scattering surfaces (i.e., ocean and vegetated land), however the application
55 to surfaces with a very complex and time-varying emissivity (such as snow cover and sea ice) required a far-away
56 more advanced algorithm taking advantage of machine learning techniques. Moreover, the algorithm is based
57 on the exploitation of an observational dataset where each ATMS multichannel observation is associated with
58 coincident (in time and space) CloudSat CPR vertical snow profile and surface snowfall rate (hereafter ATMS-
59 CPR coincidence dataset).

60 Several snowfall retrieval algorithms for cross-track scanning radiometers have evolved in the last 20 years
61 starting from the Advanced Microwave Sounder Unit-B (AMSU-B) (Zhao and Weng 2002, Kongoli et al, 2003,
62 Skofronick-Jackson et al, 2004, Noh et al, 2009, Liu and Seo 2013), and Microwave Humidity Sounder (MHS)
63 (see Liu & Seo, 2013, Edel et al, 2020), and evolving to ATMS (Kongoli et al, 2015, Meng et al, 2017, Kongoli et
64 al, 2018, You et al, 2022, Sanò et al, 2022). Some of them are based on radiative transfer simulations of observed
65 snowfall events (Kongoli et al, 2003, Skofronick-Jackson et al, 2004, Kim et al, 2008), or on in-situ data (see
66 Kongoli et al, 2015, Meng et al, 2017, Kongoli et al, 2018), others on CPR observations (Edel et al, 2020, You et
67 al, 2022, Sanò et al, 2022), or a combination of them (Noh et al, 2009, Liu & Seo, 2013).

68 The following reference has been added to the text (Line 810):

69

70 Zhao, L., & Weng, F.: Retrieval of ice cloud parameters using the Advanced Microwave Sounding Unit. *Journal*
71 *of Applied Meteorology and Climatology*, 41(4), 384-395, <https://www.jstor.org/stable/26184983>, 2002.

72

73 Reference:

74

75 Zhao, L., & Weng, F.: Retrieval of ice cloud parameters using the Advanced Microwave Sounding Unit. *Journal*
76 *of Applied Meteorology and Climatology*, 41(4), 384-395, <https://www.jstor.org/stable/26184983>, 2002.

77

78 **1.2) Line 67: replace with "new" or "latest"**

79

80 Thanks to the reviewer for the suggestion. The text has been modified

81 From:

82 *the availability of the last generation microwave radiometers*

83 to:

84 *the availability of the latest generation microwave radiometers*

85

86 **1.3) Line 89: Contrary to what's stated here, Greenland and Antarctica show scattering year-round in**
87 **window and water vapor sounding channels, and even in the low temperature sounding channels.**

88

89 Thanks to the reviewer for the comment. Greenland and Antarctica have been defined as scatter-free by
90 Grody&Basist, 1996. For what concerns our paper, the intention was to underline the absence of a significant
91 difference between the emissivities at 23 GHz and at 31 GHz, typical of the snowcover over Greenland and
92 Antarctic plateau (see Camplani et al, 2021), without referring to higher frequencies, as opposed to deep dry snow
93 at lower latitudes where this difference is evident. So we agree that the term "scatter-free" can be misleading if
94 we also consider high-frequency channels. Therefore, the text has been changed

95 from:

96 *At the same time, large areas of Greenland and Antarctica could appear as "scatter-free", although these areas*
97 *throughout the year are covered by dry snowpacks.*

98 to:

99 *At the same time, large areas of Greenland and Antarctica, although these areas are covered by dry snowpacks*
100 *throughout the year, do not show a significant difference between the two ATMS low frequency channels.*

101

102

103 References:

104 Grody, N. C., & Basist, A. N.: Global identification of snowcover using SSM/I measurements. *IEEE Transactions*
105 *on geoscience and remote sensing*, 34(1), 237-249, DOI: 10.1109/36.481908, 1996.

106
107 Camplani, A., Casella, D., Sanò, P., & Panegrossi, G.: The Passive microwave Empirical cold Surface
108 Classification Algorithm (PESCA): Application to GMI and ATMS. *Journal of Hydrometeorology*, 22(7), 1727-
109 1744, <https://doi.org/10.1175/JHM-D-20-0260.1>, 2021.

110
111 **1.4) Lines 116-119: While 2CSP is a well-recognized product and is not derived from radiative transfer**
112 **modeling, it does include assumptions about snow microphysics, and uses optimal estimation to retrieve**
113 **these parameters. The algorithm also uses a simplified radar reflectivity equation. Refer to the 2CSP ATBD**
114 **at [116 Thanks to the reviewer for the clarification. In the text, we wanted to highlight the issues inherent in using a
117 dataset based on simulations \(cloud-resolving model and radiative transfer\) with respect to one based on
118 coincident observations. The text has been changed](https://www.cloudsat.cira.colostate.edu/cloudsat-static/info/dl/2c-snow-profile/2C-SNOW-
115 PROFILE_PDICD.P1_R05.rev0_.pdf. Please modify the text here accordingly.</p></div><div data-bbox=)**

119 from:
120 *On the other side, the use of CPR-based datasets overcomes some of the limitations deriving from the assumptions*
121 *to be made in cloud-radiation model simulations (e. g., the microphysics scheme, the emissivity of the background*
122 *surface, scattering properties of ice hydrometeors), which are particularly problematic for snowfall estimation.*
123 *However, some limitations of the radar product used as reference and issues related to the spatial and temporal*
124 *matching between the CPR and the PMW radiometer measurements introduces some uncertainty.*

125 to:
126 *On the other hand, the use of CPR-based datasets overcomes some of the limitations deriving from the use of*
127 *cloud-radiation model simulations, which are particularly challenging for snowfall events. However, some*
128 *limitations of the radar product used as a reference and issues related to the spatial and temporal matching*
129 *between the CPR and the PMW radiometer measurements introduce some uncertainty. Moreover, the 2CSP*
130 *product is based on assumptions on snow microphysics, uses optimal estimation to retrieve snow parameters ,*
131 *and uses a simplified radar reflectivity equation and is affected by CloudSat CPR limitations as outlined in*
132 *Battaglia & Panegrossi, 2020.*

133
134 Reference:
135
136 Battaglia, A., & Panegrossi, G.: What can we learn from the CloudSat radiometric mode observations of snowfall
137 over the ice-free ocean?. *Remote Sensing*, 12(20), 3285, <https://doi.org/10.3390/rs12203285>, 2020.

138
139 **1.5) Line 181: How is the underestimation of heavy snowfall handled in training and validating the SWP**
140 **and SSR models?**

141 Thanks to the reviewer for the question. The aim of the algorithm is to reproduce the 2C-Snow Profile product
142 snowfall climatology, which is the only global radar product obtained from satellites. So, the underestimation has
143 not been corrected .

144 The following statement has been added to the text (line 223):
145 *Moreover, it is worth noting that CPR 2CSP product limitations for snowfall detection and estimation (see Section*
146 *2.2) affect the algorithm snowfall retrieval capabilities.*

147
148
149 **1.6) Line 273: Do the ANNs use environmental parameters? What are they?**

150 Thanks to the reviewer for the question. The final version of the algorithm does not use environmental parameters
151 as input of the ANNs, but only some ancillary parameters (Digital Elevation Model (DEM), radiometer viewing
152 angle). So the text has been modified
153 from

154 *Four ANNs are then applied to a predictor set consisting of ATMS $T_{B_{obs}}$, $\Delta T_{B_{obs-sim}}$, a surface classification
155 flag, and other environmental and ancillary parameters.*

156 to:

157 *Four ANNs are then applied to a predictor set consisting of ATMS $T_{B_{obs}}$, $\Delta T_{B_{obs-sim}}$, a surface classification
158 flag, and other ancillary parameters (elevation and ATMS viewing angle for the final version).*

159

160

161

162

163 **1.7) Lines 191-192: Add the info on the dataset's geographic area. Was the data filtered for high latitudes**
164 **given the focus of this study?**

165

166 Thanks to the reviewer for the suggestion and for the question. The data have been not filtered based on a
167 geographic criteria. However, the data selection is based on temperature ($T_{2m} < 280$ K) and water vapor content
168 ($TPW < 10$ mm) and on elevation (see lines 320-321 and *Camplani et al, 2021*); As a consequence, the majority of
169 the observations selected are obtained over high latitude areas. A statement about the dataset composition has
170 been added (see answer to Comment 1.21).

171 Reference:

172

173 Camplani, A., Casella, D., Sanò, P., & Panegrossi, G.: The Passive microwave Empirical cold Surface
174 Classification Algorithm (PESCA): Application to GMI and ATMS. *Journal of Hydrometeorology*, 22(7), 1727-
175 1744, <https://doi.org/10.1175/JHM-D-20-0260.1>, 2021.

176

177 **1.8) Lines 193-194: With a 15-min time window, the snow mass that ATMS detects in the atmosphere most**
178 **likely is higher than the near-surface snow (SSR) observed by CPR (refer to You et al., doi:**
179 **10.1029/2019GL083426). This adds uncertainties to the SSR (and to a lesser degree to SWP). Suggest the**
180 **authors run an experiment where ATMS data is collocated with CPR snowfall rate with a certain time lag**
181 **(30-minute?), and compare the retrieved ATMS snowfall rate with what is presented in this manuscript.**

182

183 Thanks to the reviewer for the suggestion. The suggested experiment is extremely interesting, and we want to take
184 it into account for future works. However, the selection of coincident observations and the making of a coincidence
185 dataset is a computationally and time consuming process, so we do not have the possibility to face this problem
186 during the revision phase. The following statement have been added to the conclusions (line 597):

187

188 *Moreover, recent studies have highlighted that TBs correlate more strongly with lagged surface precipitation*
189 *(with a time lag of 30-60 min for snowfall) than the simultaneous precipitation rate (see You et al, 2019) .*
190 *Therefore, an analysis based on a coincident dataset characterized by different time lags will be carried out. The*
191 *results of this analysis will be compared with HANDEL-ATMS performances in order to identify a way to exploit*
192 *this information to improve SSR detection and estimation.*

193

194 The following reference has been added to the text (Line 806):

195

196 *You, Y., Meng, H., Dong, J., & Rudlosky, S.: Time-lag correlation between passive microwave measurements and*
197 *surface precipitation and its impact on precipitation retrieval evaluation. *Geophysical Research Letters*, 46(14),*
198 *8415-8423, doi: 10.1029/2019GL083426, 2019.*

199

200 Reference:

201
202 You, Y., Meng, H., Dong, J., & Rudlosky, S.: Time-lag correlation between passive microwave measurements
203 and surface precipitation and its impact on precipitation retrieval evaluation. *Geophysical Research Letters*,
204 46(14), 8415-8423, doi: 10.1029/2019GL083426, 2019.

205
206 **1.9) Line 282: Is there any noticeable discontinuity in the retrieved SWP and SSR between the different**
207 **surface classes? Please add some discussion in the appropriate section.**

208
209 Thanks to the reviewer for the comment. As it is possible to observe by the case study reported, discontinuities
210 in the SWP/SSR retrieval are not observed in correspondence with the surface class change. Also for other case
211 studies analyzed it has not been observed any discontinuity in snowfall retrievals in correspondence with a surface
212 class change. In the following plots the statistical scores (POD, FAR and HSS) are reported as a function of the
213 class. It is possible to observe that there are not very large differences. Also the error statistics do not show any
214 significant difference between the various surface classes (see the answer to 1.23, Figure 9). So, the following
215 statement has been added in the section dedicated to the case study (line 525):

216 *Discontinuities in snowfall retrievals are not observed in correspondence with surface class changes.*

217
218 **1.10) Line 283: replace NASA with NOAA**

219 Thanks to the reviewer for the correction. The text has been modified

220 from:

221 *the NASA AutoSnow product*

222 to:

223 *the NOAA AutoSnow product*

224
225 **1.11) Line 290: While this is outside the scope of this study, is it possible to improve snow cover classification**
226 **using ML approach? I'd like to get the authors' comments on it.**

227 Thanks to the reviewer for the question. In *Camplani et al, 2021* a comparison between the PESCA performances
228 and the performance obtained with a RobustBoost approach (Machine Learning ensemble method) has been
229 carried out. The results show that the performances obtained with this ML approach are very similar to those
230 obtained by using PESCA. However, the leading idea of PESCA is to use a simple and not too computationally
231 demanding method to obtain a surface classification ancillary to the snowfall retrieval by exploiting the radiometer
232 low-frequency channels. Indeed, in our opinion, the use of ML approaches for the prediction of the surface
233 emissivity for snow cover surfaces is very promising. In particular, it could be of great benefit for the exploitation
234 of the heterogeneous observations from the radiometer constellation. In this context, we are presently working in
235 how the future measurements of CIMR radiometer, with an unprecedented spatial resolution, but no high
236 frequency channels, can be exploited for improving the snowfall and IWP estimates of other radiometers equipped
237 with high frequency channels, such as EPS-SG MWI, ICI, MWS the ATMS and AWS-STERNA. We sincerely
238 thank the reviewer for this comment, and we would be pleased to further discuss this topic when the revision of
239 this manuscript will be completed.

240 Reference:

241
242 Camplani, A., Casella, D., Sanò, P., & Panegrossi, G.: The Passive microwave Empirical cold Surface
243 Classification Algorithm (PESCA): Application to GMI and ATMS. *Journal of Hydrometeorology*, 22(7), 1727-
244 1744, <https://doi.org/10.1175/JHM-D-20-0260.1>, 2021.

245
246 **1.12) Line 327: give explicit definitions of POD, FAR, and HSS even though they are well known.**

247
248 Thanks to the reviewer for the suggestion. The text has been modified

249
250
251 from:

252 The statistical scores (POD, FAR, HSS) of PESCA identification of sea ice and snow cover (using AutoSnow as
253 reference) are summarized in Table 1.

254 to:

255 The statistical scores of PESCA identification of sea ice and snow cover (using AutoSnow as the reference) are
256 summarized in Table 1. In particular, the Probability of Detection (POD), the False Alarm Ratio (FAR), and the
257 Heidke Skill Score (HSS) are reported. POD, FAR, and HSS are defined by equations 2,3 and 4.

$$258 \text{POD} = \frac{h}{h+m}$$

259 (2)

$$260 \text{FAR} = \frac{f}{f+h}$$

261 (3)

$$262 \text{HSS} = \frac{2(h*cn-f*m)}{(h+m)*(m+cn)+(h+f)*(f+cn)}$$

263 (4)

264 where h represents the hits, f represents the false alarms, m represents the misses and cn represents the correct
265 negatives

266

267 **1.13) Line 346: Give reference to the radiative transfer model, or add some information about the model.**

268

269 Thanks to the reviewer for the suggestion. The simulations are based on a plane-parallel approximation (see *Ulaby,*
270 *2014*) and the gas absorption model is described by *Rosenkranz, 1998*. The text has been modified (see answer to
271 Comment 1.15).

272 The following reference has been added to the text (Line 806):

273 *Rosenkranz, P. W., Water vapor microwave continuum absorption: A comparison of measurements and models.*
274 *Radio Science, 33(4), 919-928. <https://doi.org/10.1029/98RS01182>, 1998.*

275 References:

276

277 *Ulaby, F., & Long, D., Microwave radar and radiometric remote sensing, 1st Edition, the Univ. of Michigan Press,*
278 *ISBN: 978-0-472-11935-6, 2014.*

279 *Rosenkranz, P. W., Water vapor microwave continuum absorption: A comparison of measurements and models.*
280 *Radio Science, 33(4), 919-928. <https://doi.org/10.1029/98RS01182>, 1998.*

281

282 **1.14) Line 350: Is the polarization effect on emissivity also neglected between viewing angles of 40 degree**
283 **and 52.7 degree (the max ATMS viewing angle)? Need to state it if it's the case.**

284 Thanks to the reviewer for the question. The polarization effect is less than 0.05 between 0 ° and 52.7 °, so it has
285 not been considered. In the plot below the dependence of the ocean emissivity on viewing angle at 89 GHz (top)
286 and the differences between the emissivity at nadir and the emissivity at a certain angle (bottom) are reported
287 based on the FASTEM model (see *Prigent et al, 2017*). It is possible to observe that, while the V and H emissivity
288 show a variation up to 0.15, the QV and QH emissivity variation is lower than 0.05 for scan angles < 52 °.

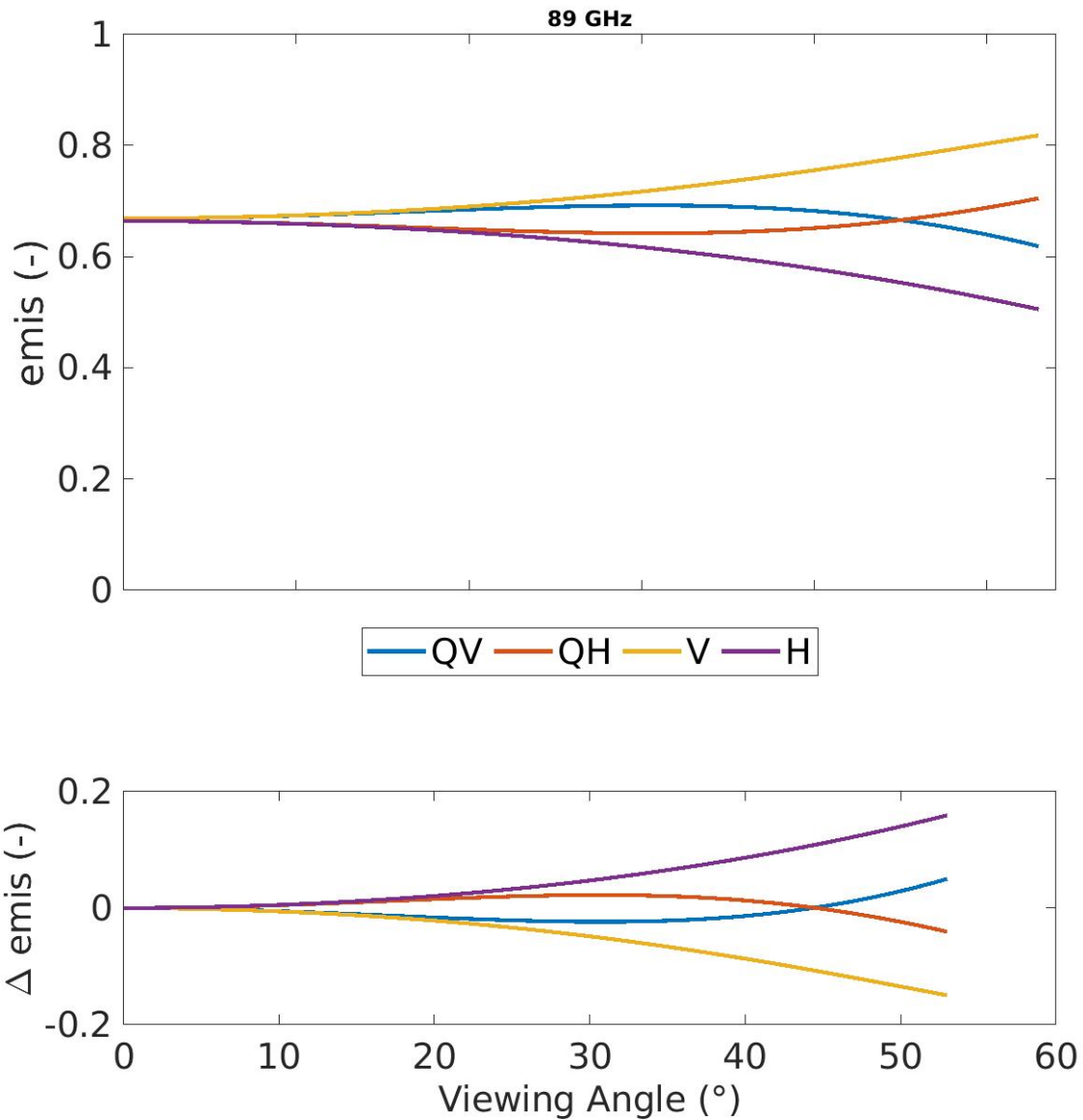
289 The text has been modified

290 from:

291 *The emissivity spectra dependence on the ATMS viewing angle for polarized surfaces has been neglected because*
292 *an analysis of such dependence in the ATMS-CPR coincidence dataset has shown that it is significant only for*
293 *larger viewing angles (tot for >40 °). This is due to the fact that cross-track scanning radiometers measure a*
294 *signal (off-nadir) which derives from a mixture between the two polarizations (e.g., quasi-vertical, QV, and quasi-*
295 *horizontal, QH). As a consequence, although the emissivities of polarized surfaces, such as open water surfaces,*
296 *are strongly influenced by the viewing angle, for the cross-track scanning radiometers the emissivity variation is*
297 *compensated by the effect of the mixture of the two polarization (see also Felde & Pickle, 1995, Prigent et al,*
298 *2000, Mathew et al, 2008, Prigent et al, 2017).*

299 to:

300 *The emissivity spectra dependence on the ATMS viewing angle for polarized surfaces has been neglected because*
301 *an analysis of such dependence in the ATMS-CPR coincidence dataset has shown that it is not significant for*
302 *ATMS viewing angles (emissivity difference smaller than 0.05 for angles up to 52.7 °). This is due to the fact that*
303 *cross-track scanning radiometers measure a signal (off-nadir) which derives from a mixture between the two*
304 *polarizations (e.g., quasi-vertical, QV, and quasi-horizontal, QH). As a consequence, although the emissivities of*
305 *polarized surfaces, such as open water surfaces, are strongly influenced by the viewing angle, for the cross-track*
306 *scanning radiometers the emissivity variation is compensated by the effect of the mixture of the two polarization*
307 *(see also Felde & Pickle, 1995, Prigent et al, 2000, Mathew et al, 2008, Prigent et al, 2017).*



308
309

Reference:

Prigent, C., Aires, F., Wang, D., Fox, S., & Harlow, C.: Sea-surface emissivity parametrization from microwaves to millimetre waves. *Quarterly Journal of the Royal Meteorological Society*, 143(702), 596-605, <https://doi.org/10.1002/qj.2953>, 2017.

310

311

312 **1.15) Line 362: Reference for the RTM?**

313 Thanks to the reviewer for the suggestion. The text has been modified

314 from:

315 *The RMSE between simulated clear-sky TBs - based on the mean emissivity values estimated for each class - and*
316 *the coincident observed clear-sky TBs appears to be too high to implement a robust signal analysis (>10 K).*

317 to:

318 *The clear-sky radiative transfer model simulations are based on the mean emissivity values estimated for each*
319 *class, and simulated by using the plane-parallel approximation (Ulaby & Long, 2014) and the Rosenkrantz gas*
320 *absorption model (Rosenkrantz, 1998) - The RMSE between simulated clear-sky TBs and the coincident observed*
321 *clear-sky TBs appears to be too high to implement a robust signal analysis (>10 K).*

322

323 References:

324 Rosenkrantz, P. W., Water vapor microwave continuum absorption: A comparison of measurements and models.
325 *Radio Science*, 33(4), 919-928. <https://doi.org/10.1029/98RS01182>, 1998.

326

327 Ulaby, F., & Long, D., Microwave radar and radiometric remote sensing, 1st Edition, the Univ. of Michigan Press,
328 ISBN: 978-0-472-11935-6, 2014.

329

330 **1.16) Line 397, the RMSE for ocean is 3.37 K in Table 2.**

331

332 Thanks to the reviewer for the observation. The text has been modified

333 from:

334 very *low RMSE values (≈ 2 K)*

335 to:

336 *low RMSE values (< 4 K)*

337

338 **1.17) Line 403: Since high frequencies are more important for snowfall retrieval, need to discuss the impact**
339 **of the significant uncertainties at these channels to retrieve SWP and SSR.**

340 Thanks to the reviewer for the suggestion. In Figure 9 (see answer to Comment 1.23) the statistical scores for
341 each PESCA class are reported. It is possible to observe that the worst scores are obtained for classes characterized
342 by high uncertainties in the clear-sky TB simulations (Perennial Snow, Winter Polar Snow). However, it is also
343 worth noting that these classes are mostly associated with environmental conditions (very dry and cold, with very
344 light snowfall events, see *Camplani et al, 2021*) which make it difficult both to obtain a more accurate clear
345 emissivity estimation and to retrieve snowfall. At the same time, it can be observed that classes characterized by
346 the highest uncertainties on the emissivity estimate (Deep Dry Snow and Broken Sea Ice), show statistical scores
347 which are coherent with the general scores of the algorithm. So it is clear that the uncertainties on emissivity
348 estimation have less influence than other factors, such as the environmental conditions.

349 The text has been modified (line 471)

350 from:

351 *In Table 6 the statistical scores of the algorithm performance by considering each PESCA class for both the SWP*
352 *and the SSR detection module are reported. It can be observed that, also considering specifically the classes where*
353 *the detection is more problematic, both for the uncertainties linked to the emissivity retrieval (see Table 2), for*
354 *the extremely dry and cold environmental conditions, and for the low intensity of the snowfall events, such as*
355 *Perennial Snow or Winter Polar Snow, HANDEL-ATMS has good detection capabilities (POD and FAR values*
356 *greater than 0.7 and less than 0.25, respectively, for both SWP and SSR). These results provide evidence that*
357 *HANDEL-ATMS can be used to analyze snowfall occurrence in the polar regions.*

358 to:

359 In Figure 9 the statistical scores of the algorithm performance by considering each PESCA class for both the
360 SWP and the SSR detection module are reported. It can be observed that, also considering specifically the classes
361 associated to extremely dry and cold environmental conditions such as Perennial Snow or Winter Polar Snow
362 (see Camplani et al, 2021) (where the detection is more problematic due to the uncertainties in the emissivity
363 retrieval (see Table 2), and to the low snowfall intensity), , HANDEL-ATMS has good detection capabilities (POD
364 and FAR values greater than 0.7 and less than 0.25, respectively, for both SWP and SSR). On the other hand, it
365 is possible to observe also that for surface classes characterized by the highest emission estimation uncertainties,
366 such as Deep Dry Snow, the statistical scores are coherent with the general scores and better than those obtained
367 in presence of extremely dry/cold environmental conditions. So, it is possible to conclude that the extremely
368 cold/dry environmental conditions - have more influence on the detection than the uncertainties on clear sky
369 emissivity estimation. Generally, these results provide evidence that HANDEL-ATMS can be used to analyze
370 snowfall occurrence in the polar regions.

371
372 Reference:

373
374 Camplani, A., Casella, D., Sanò, P., & Panegrossi, G.: The Passive microwave Empirical cold Surface
375 Classification Algorithm (PESCA): Application to GMI and ATMS. *Journal of Hydrometeorology*, 22(7), 1727-
376 1744,<https://doi.org/10.1175/JHM-D-20-0260.1>, 2021.

377
378 **1.18) Line 430: Logarithmic tangent function is not a common activation function. Please add a reference**
379 **or explain what it is.**

380 Thanks to the reviewer for this comment. It was a typo, the activation function is a sigmoid. We used hyperbolic
381 tangent and sigmoid functions, which are indeed very common activation functions. The choice of the activation
382 functions has been performed by trial and testing.

383 The manuscript has been modified

384 from:

385 *The final architecture, for all modules, is composed of four layers: an input layer with a neurons number equal*
386 *to the predictor number, and a hyperbolic tangent function as the activation function, a first hidden layer (60*
387 *neurons), and hyperbolic tangent function, a second hidden layer (30 neurons), with a logarithmic tangent*
388 *function.*

389 to:

390 *The final architecture, for all modules, is composed of four layers: an input layer with a neurons number equal*
391 *to the predictor number, and a hyperbolic tangent function as the activation function, a first hidden layer (60*
392 *neurons), and hyperbolic tangent function, a second hidden layer (30 neurons), with a sigmoid function.*

393
394 **1.19) Lines 435-436: Did the predictor set including TB_obs, TB_obs-TB_sim, and environmental variables**
395 **give better result than the set only included the first two? If not, why? Is it because TB_sim also used the**
396 **environmental variables being tested?**

397 Thanks to the reviewer for the question. The NNs that use both the $\Delta_{obs-sim}$ and the environmental parameters show
398 detection scores almost equal to those obtained by using only $\Delta_{obs-sim}$. This is because the information about
399 environmental conditions is already used as input in the clear-sky TB simulations The following statement has
400 been added to the text (line 438):

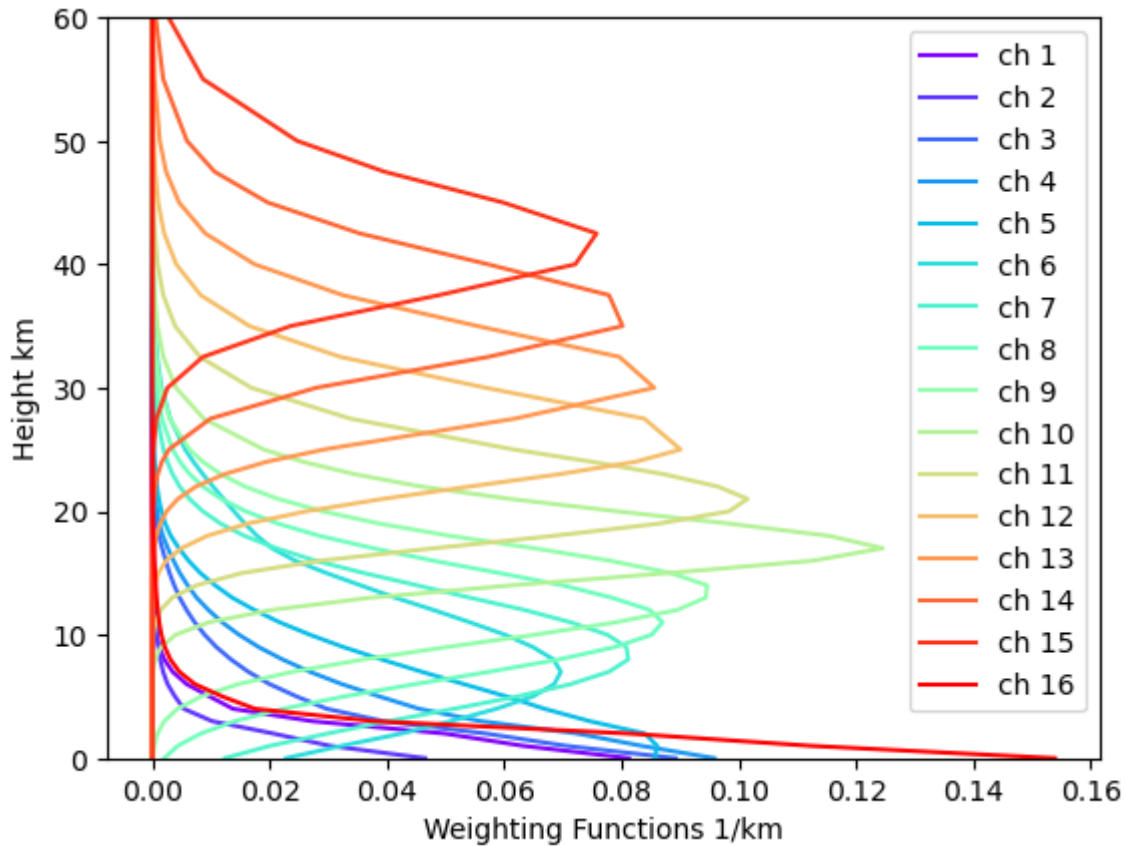
401 *On the contrary, the simultaneous use of both the $\Delta TB_{obs-sim}$ and the environmental parameters show scores almost*
402 *equal to that obtained by using only $\Delta TB_{obs-sim}$.*

403
404
405
406

1.20) Lines 444: Which 16 ATMS channels and how are they selected?

407 Thanks to the reviewer for the suggestion. The sixteen channels are ATMS channels 1-9, 16-22. The ATMS 10-
408 15 channels peak above the tropopause, so we did not take them into account in the development of HANDEL-

409 ATMS. Figure below shows the temperature weighting functions for a standard atmosphere in clear sky
410 conditions.



411

412 The text has been modified

413 from:

414 *16 ATMS TB_{obs}*

415 to:

416 *1-9, 16-22 ATMS channels TB_{obs} (the 10-15 ATMS channels have not been considered because their weighting*
417 *function peaks above the tropopause).*

418

419 **1.21) Section 4.1: Some details about the validation data should be provided. Is the data from selected**
420 **snowfall events used or from a time period? How many events were included and their geographic areas?**
421 **How many data points were in the dataset etc.? The information is important because it provides the**
422 **context for the performance metrics.**

423 Thanks to the reviewer for the suggestion. The following section has been added to the text of section 2.3 (line
424 223):

425 *In this work, the dataset has been filtered based on humidity ($TPW < 10$ mm) and temperature ($T_{2m} < 280$ K) and*
426 *elevation conditions (the working limits of the PESCA algorithm, see Camplani et al, 2021) leading to a good*
427 *representation of the higher latitudes with 80 % of the dataset elements located above $60^{\circ}N/S$. The dataset is*
428 *made of $2,14 \cdot 10^6$ elements, including $1,07 \cdot 10^6$ elements with falling snow ($2CSP$ $SWP > 0$ $kg\ m^{-2}$) and $9,99 \cdot 10$*
429 *5 with snowfall at the surface ($2CSP$ $SSR > 0$ $mm\ h^{-1}$) . The training and test phases have been conducted by*
430 *splitting randomly the dataset, with $\frac{1}{3}$ of the elements in the training and $\frac{2}{3}$ of the elements in the test dataset.*

431

432 Reference:

433

434 Camplani, A., Casella, D., Sanò, P., & Panegrossi, G.: The Passive microwave Empirical cold Surface
435 Classification Algorithm (PESCA): Application to GMI and ATMS. *Journal of Hydrometeorology*, 22(7), 1727-
436 1744,<https://doi.org/10.1175/JHM-D-20-0260.1>, 2021.

437
438

439 **1.22) Line 451: A large percentage of the snowfall appears to fall when T_2m is around the freezing point**
440 **or higher. Snowfall under such conditions generally has different characteristics from snowfall in high**
441 **latitudes which is the focus of this study. Add some discussion about the data distribution and its impact on**
442 **the new snowfall algorithm.**

443 Thanks to the reviewer for the suggestion. Generally, the SWP detection shows better performances in moister
444 and warmer conditions than in colder/drier situations for two main reasons: 1) the atmosphere is less transparent
445 2) these conditions are usually associated with more intense events. However, in these conditions there can be a
446 mismatch between the presence of falling snow in the atmosphere and the presence of snowfall at the surface;
447 therefore, the SSR detection statistical scores show a maximum around 273 K and 5 mm and then decrease. From
448 Figure 8, it is possible to observe that the maximum number of observations and of snowfall elements in the
449 dataset is around 273 K, where the best performances are obtained. However, it is worth noticing that HANDEL
450 shows very good results also in very dry and very cold conditions. We believe that this is the main achievement
451 of this work, since the main objective of this study is to show that HANDEL is able to detect and retrieve snow
452 also in extreme conditions typical of the higher latitudes. We think that this is the added value of this study. In
453 order to highlight this aspect, we have added a new figure showing the variability of the estimation statistical
454 scores and the mean SWP and SSR with TPW (see answer to Comment 1.25).

455

456 **1.23) Line 471: Add HSS to Table 6.**

457

458 Thanks to the reviewer for the suggestion.

459 We have deleted Table 6 and we have added Figure 9, where the POD, FAR, HSS, the observation occurrences
460 and the snowfall observation occurrences (SWP, SSR>0) are reported.

461

462

463

464

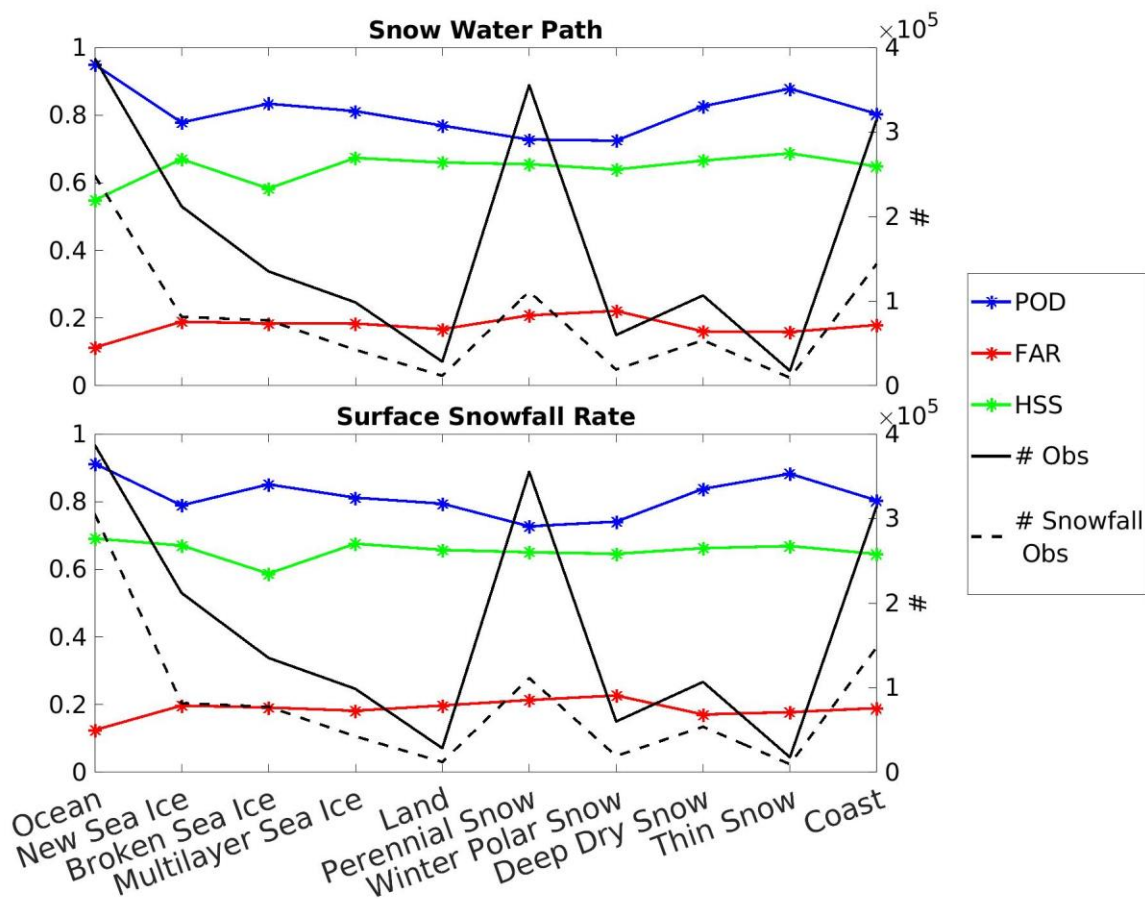


Figure 9: Same as Figure 7 but for PESCA surface classes.

465
466
467

1.24) Table 5: Since the goal of this study is to retrieve snowfall in high latitude, it'd be informative to analyze how well the statistics represent the cold, dry and light snowfall versus the warm, moist, and heavier snowfall. Please add some quantitative analysis to show the performance of the snowfall representative of high latitude conditions.

472 Thanks to the reviewer for the suggestion. The dependence of the detection scores on the environmental conditions has been reported in Figure 7 and in Figure 8. The presence of a less transparent atmosphere and the presence of high SWP values generates a more intense signal. We have decided to add one Figure in the manuscript showing the variability of the snowfall estimation statistical scores, as well as SWP and SSR, with TPW (see answer to Comment 1.25).

477

1.25) Line 487: Typically, high latitude snowfall is rather light. Does this result mean that the snowfall retrieval in high latitude is generally overestimated? Add some discussion here.

480 Thanks to the reviewer for the comment. From Figure 9 it is possible to observe that the algorithm tends to overestimate light snowfall, while there is a better agreement for more intense snowfall. Very light snowfall events are linked to the dry /cold environmental conditions typical of high latitude areas, where more intense snowfall events are typical of moister conditions. We state that "Generally, it can be observed that, although HANDEL-ATMS is able to detect extremely light snowfall events, it does not have the sensitivity to correctly estimate their intensity." The final part of Section 4.1 has been largely modified (see below)

486 We decided to add the following Figure to the paper in order to answer 1.22, 1.24 and 1.25.

487

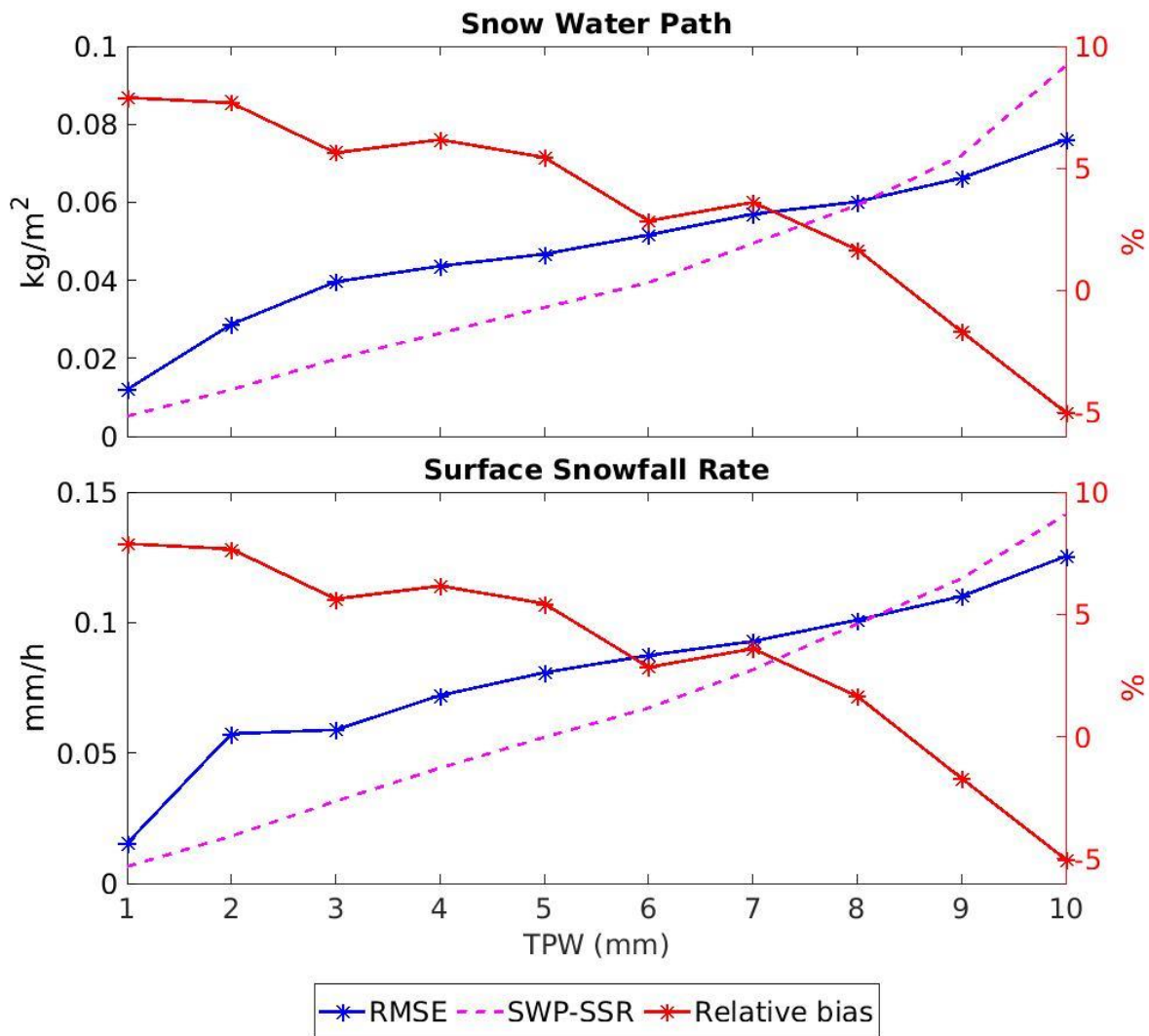


Figure 11: HANDEL-ATMS SWP and SSR Detection Performances for different bins of TPW. The left y-axis reports RMSE absolute values and the mean intensity value for each 1-mm TPW bin, while the relative bias, calculated as the ratio between the bias and the SWP/SSR mean value for each bin.

488
489
490
491
492
493
494

495 The text has been modified to comment the Figure 11 (Line 488)

496 from:

497 . Generally, it can be observed that, although HANDEL-ATMS is able to detect extremely light snowfall events, it
498 does not have the sensitivity to correctly estimate their intensity.

499
500 to:

501
502 Figure 11 shows the dependence of HANDEL-ATMS snowfall estimation error statistics, as well of SWP and SSR,
503 on TPW. The curves represent the mean SWP or SSR computed for each 1-mm TPW bin, the RMSE and the relative
504 bias (the ratio between the bias and the SWP/SSR mean value for each bin). TPW and snowfall intensity are
505 strongly correlated. An increase of the absolute RMSE can be observed as TPW increases, and it is larger than
506 the SWP/SSR mean value for TPW < 8 mm. A similar behavior can be observed by analyzing the dependence of

507 *HANDEL-ATMS snowfall estimation error statistics on T_{2m} (not shown). A very moderate overestimation is*
508 *observed for $TPW < 8$ mm and for lower SWP and SSR values (< 0.1 mm/h), with relative bias around 5%, (up*
509 *to 8% only for extremely low TPW values and very low number of observations (see Figure 7)), while*
510 *underestimation (relative bias up to -5%) is observed for higher TPW values and higher SWP and SSR values.*
511 *Generally, light snowfall events are linked to the very cold/dry environmental conditions typical of high-latitude*
512 *regions. So, the algorithm manages to detect also the very light snowfall typical of high latitudes, but tends to*
513 *slightly overestimate snowfall intensity in such conditions. It can be concluded that HANDEL-ATMS has good*
514 *detection capabilities (also for extremely light snowfall) but it shows some limitations in correctly estimating its*
515 *intensity, with slight overestimation of the very light snowfall typical of high latitudes.*

516

517 **1.26) Lines 555-558: See the comment on line 27.**

518

519 Thanks to the reviewer for the suggestion. The text has been modified

520 from:

521

522 *The driving and innovative principle in the algorithm development is the exploitation of the full range of ATMS*
523 *channel frequencies to characterize the frozen background surface radiative properties at the time of the overpass*
524 *to be able to better isolate and interpret the snowfall-related contribution to the measured multi-channel upwelling*
525 *radiation.*

526 to

527

528 *The driving and innovative principle in the algorithm development is the exploitation of the full range of ATMS*
529 *channel frequencies to characterize the frozen background surface radiative properties at the time of the overpass*
530 *to be able to better isolate and interpret the snowfall-related contribution to the measured multi-channel upwelling*
531 *radiation. A similar approach has been used by Zhao & Weng, 2002; however, their application was limited to*
532 *non-scattering surfaces and was based on empirical relationships.*

533

534 Reference:

535

536 Zhao, L., & Weng, F.: Retrieval of ice cloud parameters using the Advanced Microwave Sounding Unit. *Journal*
537 *of Applied Meteorology and Climatology*, 41(4), 384-395, <https://www.jstor.org/stable/26184983>, 2002.

538

539

Reviewer 2

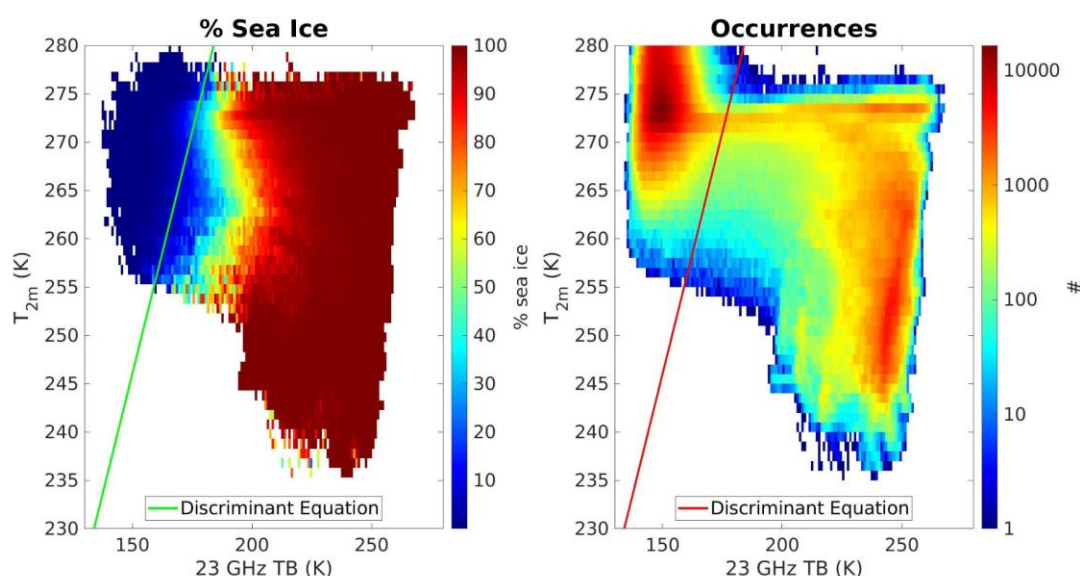
540
541 We would like to thank Reviewer #2 for his/her review of our paper and the important comments and suggestions
542 provided. Please, find below our responses to the Reviewer's comments and the details on how we address them
543 in the new version of the manuscript

544 **General comments.**

545 **The text is a bit hard to follow. It is highly recommended that the authors make an effort to shorten it and**
546 **make the language and the message more succinct. The quality of the figures can be significantly improved**
547 **as well. There are a few important points that need to be cleared in the next revision.**

548 Thanks to the reviewer for the suggestion. We have shortened the manuscript and tried to make the message more
549 succinct. We have also improved figures 2, 6, 7, 8, 11, and 14 (now Figures 13 and 16 because new Figures 9
550 and 11 have been added to address some comments by Reviewer 1) and the captions have been modified
551 accordingly.

552 Figure 2:



553

554 The caption has been changed

555 from:

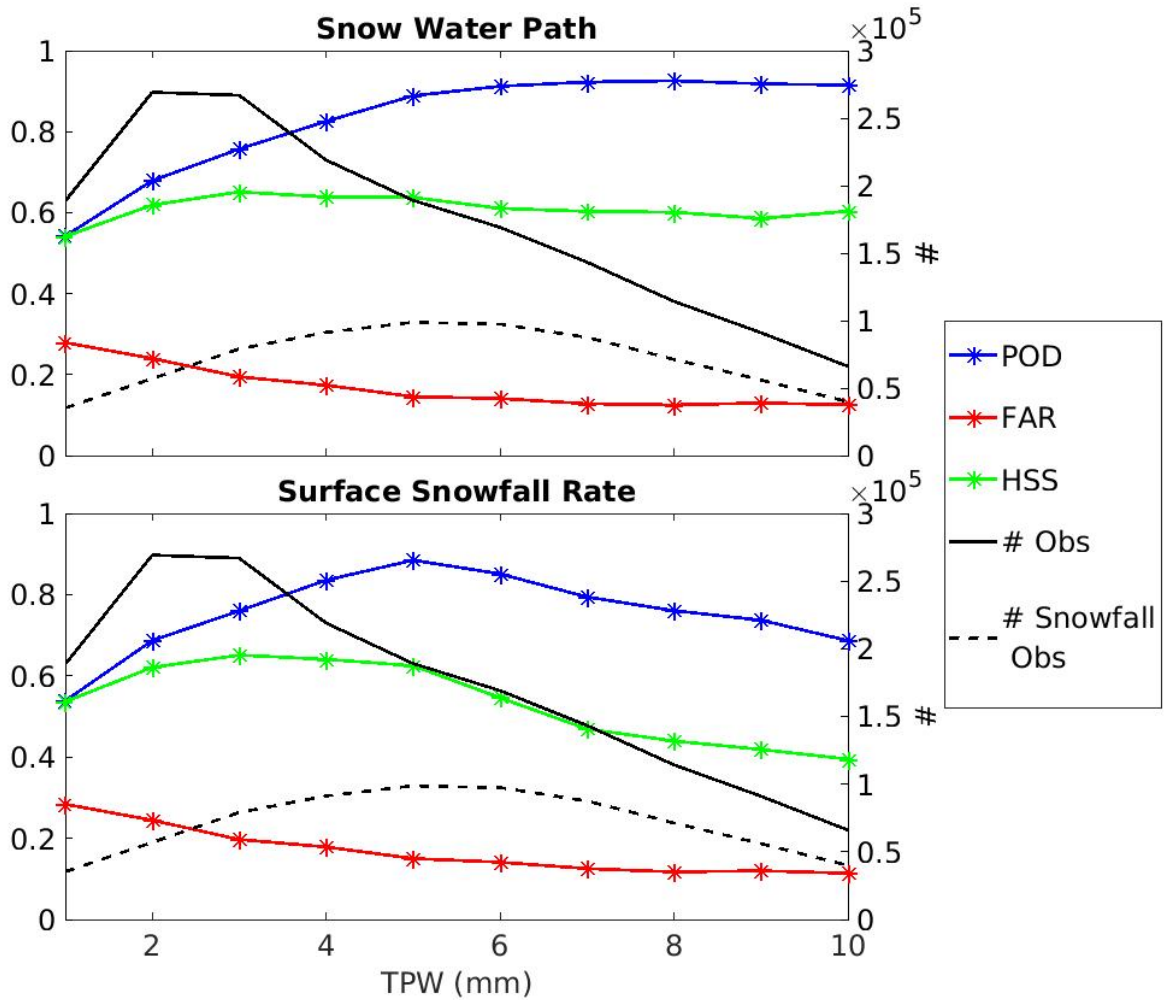
556 *Figure 2: Sea Ice Detection: 23 TB- T_{2m} Plan. The color represents the mean AutoSnow sea ice percentage within each bin*
557 *(left) and the observation occurrence (right).*

558
559 to
560 *Figure 2: Sea Ice Detection: 23 TB- T_{2m} Plan. The color represents the mean AutoSnow sea ice percentage within each bin*
561 *(left) and the observation occurrence (right). The green (left) and red (right) lines represent the discriminant Equation*
562 *between sea ice and ocean.*

563

564 For Figure 6, see answer to Comment 2.20.

565



567

568

569 The caption has been changed

570 from:

571 *Figure 7 HANDEL-ATMS SWP and SSR Detection Performances for different bins of TPW. The left y-axis*
 572 *reports POD, FAR and HSS vales, while the right y-axis reports the total number and snowfall observations in*
 573 *the dataset. POD-tot, FAR-tot and HSS-tot (dotted lines) represent the statistical scores estimated on the total*
 574 *dataset (values reported in Table 2).*

575

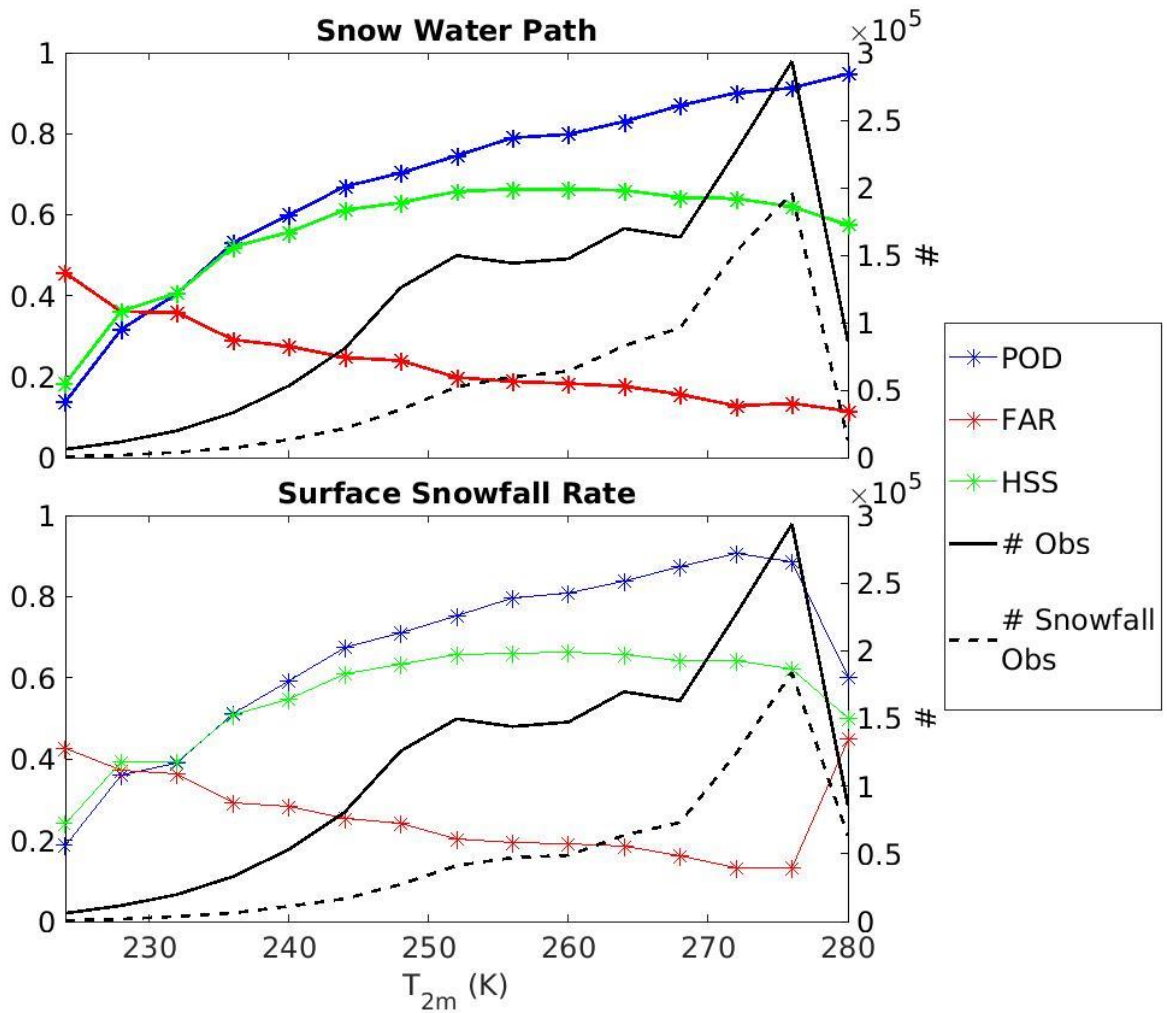
576

577 to

578 *Figure 7: HANDEL-ATMS SWP and SSR Detection Performances for different bins of TPW. The left y-axis*
 579 *reports POD, FAR and HSS vales, while the right y-axis reports the total number and snowfall observations in*
 580 *the dataset.*

581

582 Figure 8:



583

584

585

586 The caption has not been changed

587

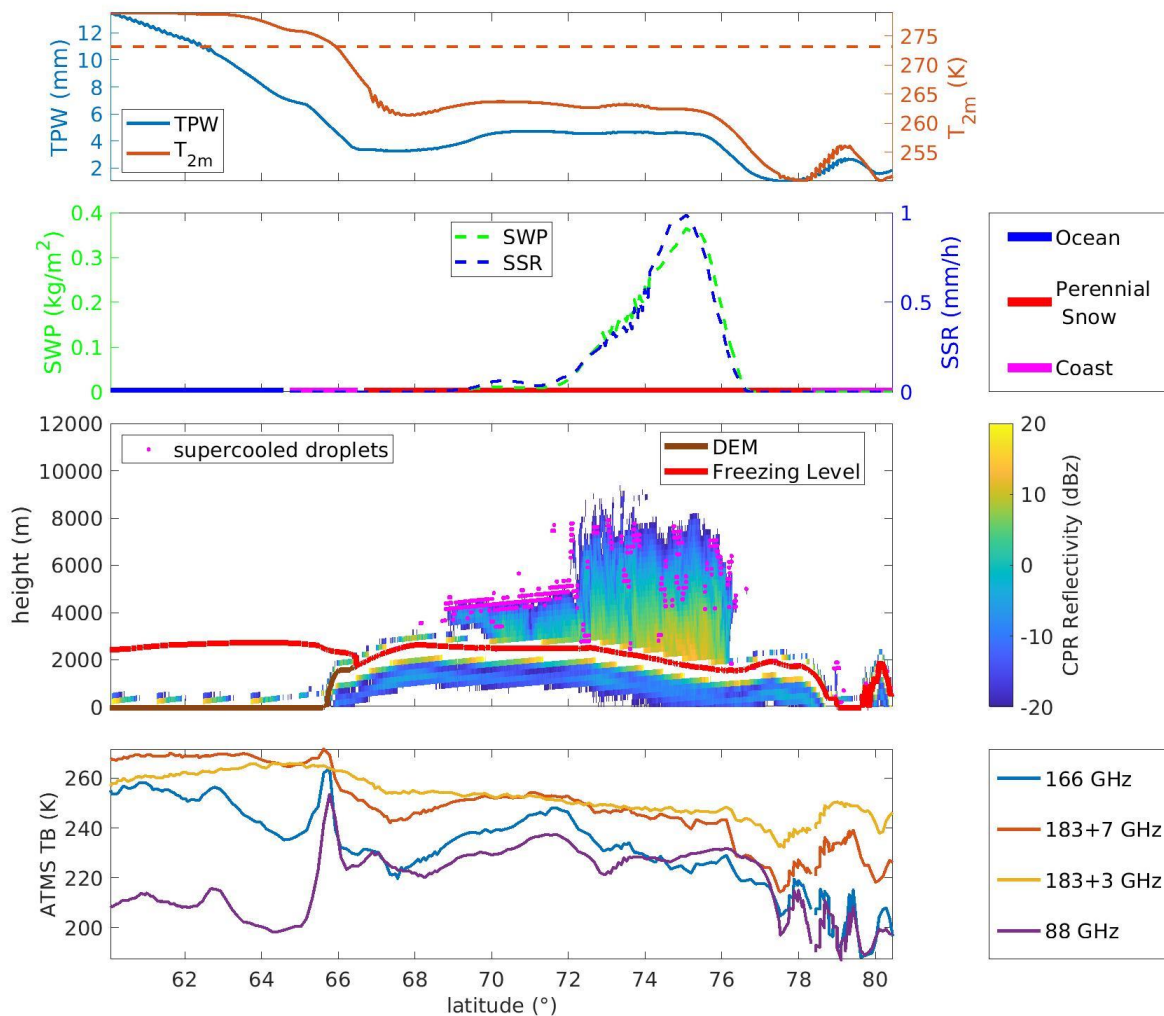
588

589

590

591

592



594

595 The caption has been changed

596 from:

597 *Figure 11: Greenland - 2016/04/24 - Synopsis along CloudSat Track. The first panel shows the ECMWF TPW*
 598 *and T_{2m} values along the CloudSat track. In the second panel, the 2CSP SWP (left) and the SSR (right)*
 599 *values are reported, besides the PESCA classification along CloudSat track. In the third panel, the CPR reflectivity*
 600 *(values are reported in the colorbar below), the supercooled water droplets detected by DARDAR (magenta points)*
 601 *are shown. Also the Digital Elevation Model (brown line) and the ECMWF Freezing Level (red line) along*
 602 *CloudSat track are reported. In the bottom panel the observed TBs of the main high-frequency channels (88 GHz,*
 603 *166 GHz, 183+3 GHz, 183+7 GHz) along CloudSat track are shown.*

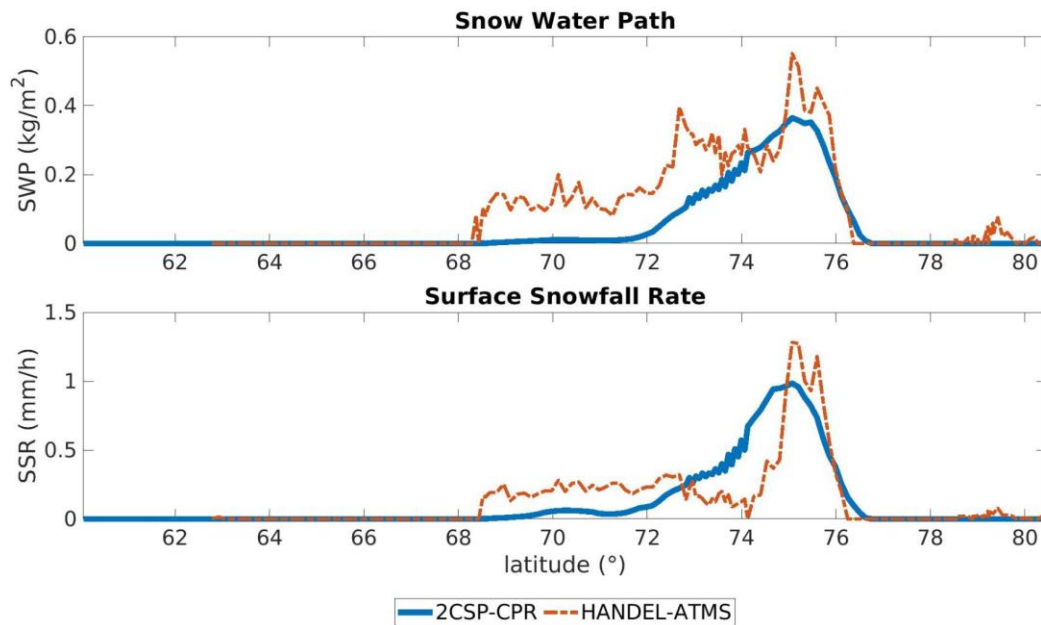
604

605

606 to

607 *Figure 13: Greenland - 2016/04/24 - Synopsis along CloudSat Track. The first panel shows the ECMWF TPW*
 608 *and T_{2m} values along the CloudSat track. In the second panel, the 2CSP SWP (left) and the SSR (right)*
 609 *values are reported, besides the PESCA classification along CloudSat track. In the third panel, the CPR reflectivity*
 610 *(values are reported in the colorbar on the right), the supercooled water droplets detected by DARDAR (magenta*
 611 *points) are shown. Also the Digital Elevation Model (brown line) and the ECMWF Freezing Level (red line)*
 612 *along CloudSat track are reported. In the bottom panel the observed TBs of the main high-frequency channels*
 613 *(88 GHz, 166 GHz, 183+3 GHz, 183+7 GHz) along CloudSat track are shown.*

614 Figure 14/16:



615

616 The caption has not been changed

617 For the new Figures 9 and 11, see answers to Comments 2.5 and 2.18.

618 **2.1) The explanation of the inverse radiative transfer modeling is missing. Such an inversion can be**
619 **significantly underconstrained and add additional uncertainty to the results.**

620 Thanks to the reviewer for the comment. The model used is a plane-parallel approximation (see *Ulaby&Long,*
621 *2014*); the gas absorption model is that described by *Rosenkranz, 1998*. In particular, the emissivity has been
622 calculated by inverting the radiative transfer equation

623
$$TB = T_{up} + (1 - \varepsilon) * T_{down} * e^{-\tau} + \varepsilon * T_{skin} * e^{-\tau}$$

624 to

625
$$\varepsilon = \frac{TB - T_{up} - T_{down} * e^{-\tau}}{e^{-\tau} * (T_{skin} - T_{down})}$$

626 where T_{up} represents atmospheric upward emission, T_{down} represents the atmospheric downward emission, τ
627 represents the atmospheric optical thickness, ε represents the emissivity, T_{skin} represents the skin temperature and
628 TB the ATMS observed TB. T_{up} , T_{down} , and τ are obtained by applying the Rosenkranz model using ECMWF-
629 AUX temperature and water vapour profiles, T_{skin} is obtained from ECMWF-AUX product.

630

631 References:

632 Rosenkranz, P. W., Water vapor microwave continuum absorption: A comparison of measurements and models.
633 *Radio Science*, 33(4), 919-928. <https://doi.org/10.1029/98RS01182>, 1998.

634

635 Ulaby, F., & Long, D., Microwave radar and radiometric remote sensing, 1st Edition, the Univ. of Michigan Press,
636 ISBN: 978-0-472-11935-6, 2014.

637 **2.2) Please clarify upfront whether the estimated values of surface emissivities are used dynamically or**
638 **statistically in the algorithm. Do they change in time or not?**

639 Thanks to the reviewer for the comment. The emissivity values are retrieved for each pixel using the low-
640 frequency TBs and environmental parameters at the time of the overpass; therefore, the emissivities are used
641 dynamically. So the text has been changed:

642 Line 27:

643 from:

644 *Moreover, their wide range of channel frequencies (from 23 GHz to 190 GHz), allows for the radiometric*
645 *characterization of the surface at the time of the overpass along with the exploitation of the high-frequency*
646 *channels for snowfall retrieval.*

647 to:

648 *Moreover, their wide range of channel frequencies (from 23 GHz to 190 GHz), allows for the dynamic radiometric*
649 *characterization of the surface at the time of the overpass along with the exploitation of the high-frequency*
650 *channels for snowfall retrieval.*

651

652 Line 136:

653 from:

654 *The present work has the aim to develop an algorithm for snowfall detection and estimation by exploiting the*
655 *large frequency range typical of the last generation radiometers and to obtain a radiometric characterization of*
656 *the background surface at the time of the satellite overpass in order to highlight the complex relationship between*
657 *upwelling radiation and snowfall signature, which makes the detection very difficult in the typical conditions of*
658 *the high latitudes.*

659 to:

660 *The present work has the aim to develop an algorithm for snowfall detection and estimation by exploiting the*
661 *large frequency range typical of the last generation radiometers and to obtain a dynamic radiometric*
662 *characterization of the background surface at the time of the satellite overpass in order to highlight the complex*
663 *relationship between upwelling radiation and snowfall signature, which makes the detection very difficult in the*
664 *typical conditions of the high latitudes.*

665

666 **2.3) It will be helpful if the authors clarify why we need land surface classification for the algorithm. For**
667 **example, there are multiple products for the detection of the presence of snow and sea ice dynamics using**
668 **optical bands (every 30 minutes). These optical products can be more accurate than microwave**
669 **classification schemes, in terms of the presence or absence of frozen surfaces. Why we should not use them?**

670 Thanks to the reviewer for the question. There are indeed multiple products for snow-cover and sea ice detection.
671 However, PESCA aim is to obtain information ancillary to the snowfall retrieval at the time of the overpass, by
672 exploiting the same instruments and the same type of data which will be used downstream for snowfall retrieval
673 (see *Camplani et al, 2021*). We are more interested in the emissivity spectrum in the microwave than in very
674 accurate and high-resolution snow and sea ice detection. Moreover, products based on optical observations are
675 unreliable in presence of clouds, while our goal is to use them to retrieve cloud properties. To our knowledge, the
676 only product available every 30 min comes from geostationary satellites that show several limitations in observing
677 high latitudes.

678

679 References:

680 Camplani, A., Casella, D., Sanò, P., & Panegrossi, G.: The Passive microwave Empirical cold Surface
681 Classification Algorithm (PESCA): Application to GMI and ATMS. *Journal of Hydrometeorology*, 22(7), 1727-
682 1744,<https://doi.org/10.1175/JHM-D-20-0260.1>, 2021.

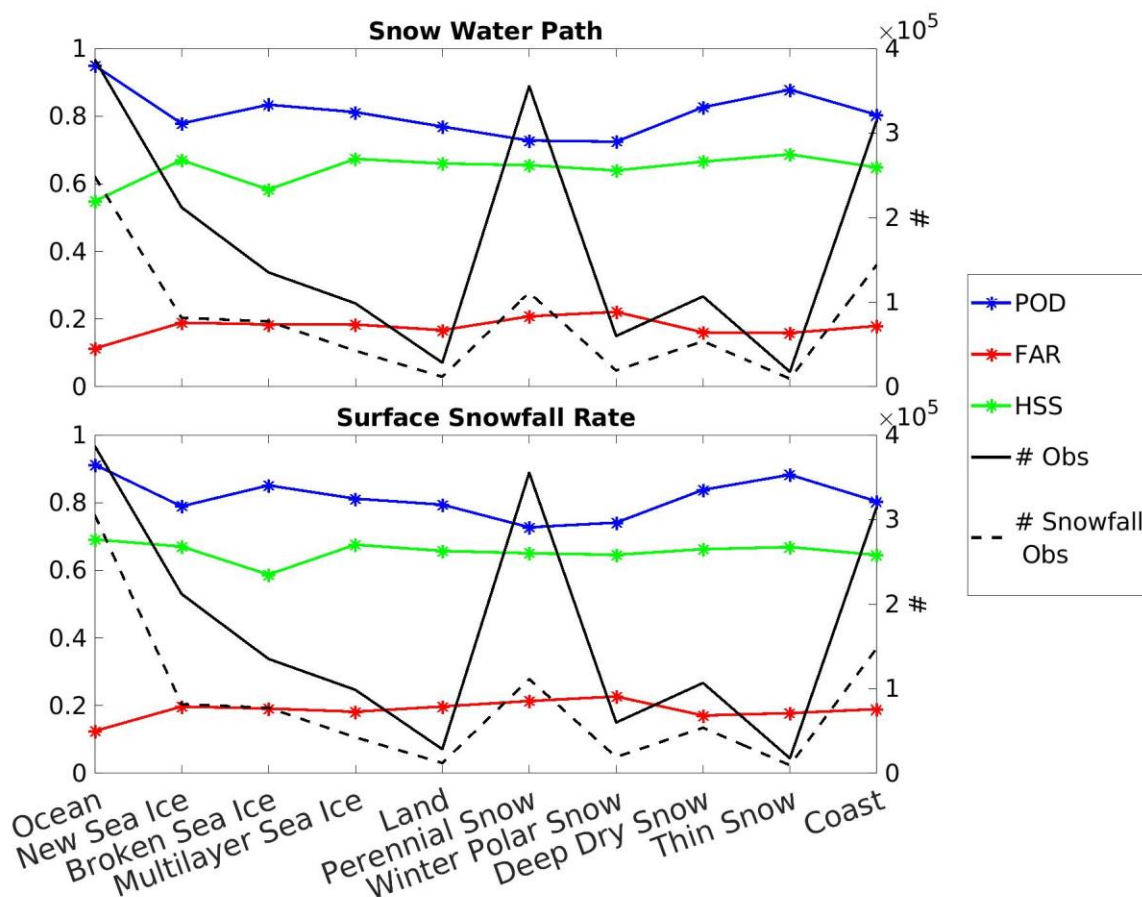
683 **2.4) From a methodological standpoint, the explanations of neural networks need to be improved. A the**
684 **same time, the use of linear discriminant analysis seems outdated in light of the new deep-learning**
685 **classification models.**

686 Thanks to the reviewer for the comment. We know that deep-learning classification models are more effective
 687 than models based on other machine learning approaches, such as linear discriminant analysis. However, our goal
 688 was to obtain a classification scheme preliminary to the snowfall retrieval modules, and so we have chosen to use
 689 methods which are simple and not too computationally and time consuming.

690

691 **2.5) While the paper focuses on different land surface types and sea ice ages, it is unclear how statistically**
 692 **significant the presented results are in Table 7. The number of training and testing samples needs to be**
 693 **clarified.**

694 Thanks to the reviewer for the suggestion. We believe that the reviewer is referring to Table 6. We have replaced
 695 it with Figure 9. In the two plots the statistical scores for each class, the total observation number and the snowfall
 696 observation number for the test phase are reported. For what concerns the number of training and testing samples,
 697 see answer to Comment 2.6.



698
 699 **Figure 9: Same as Figure 7 but for PESCA surface classes.**

700

701

702 The violet continuous and dashed line represents the total class occurrence and the snowfall occurrence for each
 703 class respectively. So, it is possible to observe that also the less populated classes, such as Thin Snow, are
 704 characterized by about 3×10^4 total observations and 1×10^4 snowfall observations. So the statistics can be
 705 considered statistically significant. This Figure has been added to the manuscript.

706 **2.6) It would benefit the paper if the authors provide the entire confusion matrix of the detection of snowfall,**
707 **including, recall, precision, and accuracy.**

708 Thanks to the reviewer for the suggestion. Here the confusion matrices and the precision, recall and accuracy
709 values are reported.

710

SWP detection - Confusion Matrix		
HANDEL/2CSP	YES	NO
YES	606711	106407
NO	106541	581671

711 precision=0.85

712 recall=0.85

713 accuracy=0,84

714

SSR detection - Confusion Matrix		
HANDEL/2CSP	YES	NO
YES	541688	102542
NO	113615	643485

715 precision=0.82

716 recall=0.84

717 accuracy=0,84

718 The total number of observations is $1,40 \cdot 10^6$, which corresponds to about $\frac{2}{3}$ of the total observations number. A
719 similar proportion can be observed for the SWP and SSR observations. The following statement has been added
720 to the text (line 223):

721 *In this work, the dataset has been filtered based on humidity ($TPW < 10$ mm) and temperature ($T_{2m} < 280$ K)*
722 *conditions (the working limits of the PESCA algorithm, see Camplani et al, 2021) leading to a good*
723 *representation of the higher latitudes with 80 % of the dataset elements located above $60^\circ N/S$. are . The dataset*
724 *is made of $2,14 \cdot 10^6$ elements, including $1,07 \cdot 10^6$ elements with falling snow ($2CSP\ SWP > kg/m^2$) and $9,99 \cdot 10$*
725 *5 with snowfall at the surface ($2CSP\ SSR > 0$ mm/h) . The training and test phases have been conducted by splitting*
726 *randomly the dataset, with $\frac{1}{3}$ of the elements in the training and $\frac{2}{3}$ of the elements in the test dataset.*

727 Therefore, data about the dataset dimension, the training and test phase and the snowfall have been added to the
728 text. We would prefer not to add the confusion matrices to the text in order to avoid further lengthening the
729 manuscript. We think that the information about the dataset, joined with the statistical scores, shows a

730 comprehensive picture of the study. At the same time, the recall gives the same information of POD, and precision
731 can be considered the complementary value to 1 of the FAR. The information linked to the accuracy can be
732 misleading: so we would prefer to keep in the text only the information about POD, FAR and HSS.

733 **Detail comments:**

734 **2.7) Section 2.4 is long and has some generic explanations about for example neural networks, which is not**
735 **necessary at this time. It is recommended to shorten the text.**

736 Agreed. The text has been shortened (see answer to Comment 2.8).

737 **2.8) The explanation of the architecture of the neural network is weak. First of all the networks use the**
738 **Levenberg-Marquardt algorithm which is extremely old and is not being used in modern training of deep**
739 **neural networks. Unlike algorithms like Adam, it is prone to get stuck in local minima and suffer from the**
740 **vanishing gradient problem.**

741 We agree with the reviewer that the LM algorithm is outdated and it is not being used in deep neural network
742 training. Our point here is that our networks are shallow, as written in section 3.2 of the manuscript:

743
744 *The snowfall detection and estimation modules have been based on ANNs. Four ANNs have been developed: two*
745 *for the detection of SWP and SSR and two for the SWP and SSR estimate. The performance of more than 50*
746 *architectures have been tested, by varying the number of layers, the number of neurons for each layer, and the*
747 *activation functions. The final architecture, for all modules, is composed of four layers: an input layer with a*
748 *neurons number equal to the predictor number, and a hyperbolic tangent function as the activation function, a*
749 *first hidden layer (60 neurons), and hyperbolic tangent function, a second hidden layer (30 neurons), with a*
750 *logarithmic tangent function.*

751
752 Therefore, the neural networks described in this paper are composed of less than 150 weights. These networks fall
753 into the category of feed forward, or multilayer perceptron networks, or shallow neural networks. The LM
754 optimizer is prone to several issues when the depth of the network grows (i.e. if the number of weights to be
755 trained is higher than about 500, see *Yu & Wilamowski, 2018*), such as gradient vanishing, however it has been
756 proven to be a very accurate optimizer for shallow neural networks. The use of the LM optimizer forces the choice
757 of the error function, that needs to be the mean squared error, in regression problems, and may result slower than
758 other optimizers, however it has proven to reach higher accuracy in many problems, even in very recent papers,
759 in particular we followed the *Hagan&Menhaj, 1994* implementation of the LM algorithm that has been cited in
760 about 700 papers after 2022 (see the google scholar link to recent citation of this paper). Moreover, we did test
761 the impact of the choice of the optimizer for one of the neural networks module of the HANDEL-ATMS algorithm,
762 and the results confirmed the use of the LM optimizer as an optimal choice for the complexity of the networks
763 that we are training and for the size of the dataset that we are using. In particular the LM optimizer resulted to be
764 more accurate but slower than other optimizers (including the Conjugate-gradient, gradient descend with
765 momentum and Adam optimizers).

766
767 About the first point raised by the reviewer “The explanation of the architecture of the neural network is weak”,
768 we believe that He/She is referring to section 2.4.1, that was intended as a brief introduction, and that has been
769 modified

770
771
772
773
774
775
776

from:

777 **2.4.1 Artificial Neural Networks**

778 An Artificial Neural Network (ANN) is an information-processing system inspired by the functioning of biological
779 neural networks. It is composed of neurons, i. e., elements where the information is processed using an activation
780 function, and the connecting links between the neurons, where a weight multiplies the deriving from the upstream
781 signal. In particular, the HANDEL-ATMS snowfall detection and estimation modules have been developed using
782 feedforward multilayer neural network architectures, i. e., a neural network architecture where the neurons are
783 arranged in layers; each neuron belonging to a layer receives, as input to its transfer function, a weighted sum of
784 the outputs of the previous layer. This architecture, which is defined by the number of layers, the number of
785 neurons for each layer, and the transfer function of each neuron, has to be designed beforehand. The weights of
786 connection links and the bias values for each layer are estimated with a training process, based on the Levenberg–
787 Marquardt algorithm (see Sanò et al, 2015)

788 to:

789 **2.4.1 Artificial Neural Networks**

790 The HANDEL-ATMS snowfall detection and estimation modules have been developed using feedforward
791 multilayer neural network architectures, i. e., a neural network architecture where the neurons are arranged in
792 layers. This architecture, which is defined by the number of layers, the number of neurons for each layer, and the
793 transfer function of each neuron, has to be designed beforehand. The weights of connection links and the bias
794 values for each layer are estimated with a training process, based on the Levenberg–Marquardt algorithm (see
795 Sanò et al, 2015). The specific networks architecture, and the training and optimization procedure of the
796 HANDEL-ATMS algorithm are described in detail in section 3.2.

797

798 References:

799

800 Yu, H., & Wilamowski, B. M.: Levenberg–marquardt training. In *Intelligent systems* (pp. 12-1), CRC Press, ISBN
801 9781315218427, 2018.

802

803 Hagan, M. T., & Menhaj, M. B.: Training feedforward networks with the Marquardt algorithm, *IEEE transactions*
804 *on Neural Networks*, 5(6), 989-993, DOI: [10.1109/72.329697](https://doi.org/10.1109/72.329697), 1994.

805

806 **2.9) Line 424–445 It is unclear how the detection and estimation networks are implemented. What are the**
807 **cost functions? This must be clarified.**

808 Thanks to the reviewer for the suggestion. The cost function is a sum of squares error (SSE) given by the following
809 equation:

810
$$E = \frac{1}{n} \sum_{i=1}^n (y_i - t_i)^2$$

811 where y represents the output of the neural networks, and t represents the reference truth value. The characteristics
812 of this Neural network approach have been largely described by Sanò et al, 2015, doi:10.5194/amt-8-837-2015).

813 So, a reference to this paper has been added (line 431):

814 (for more information about the Neural Network characteristics, see Sanò et al, 2015)

815

816 References:

817

818 Sanò, P., Panegrossi, G., Casella, D., Di Paola, F., Milani, L., Mugnai, A., Petracca, M., & Dietrich, S.: The
819 Passive microwave Neural network Precipitation Retrieval (PNPR) algorithm for AMSU/MHS observations:
820 description and application to European case studies. *Atmospheric Measurement Techniques*, 8(2), 837-857,
821 <https://doi.org/10.5194/amt-8-837-2015>, 2015.

822

823 **2.10) Line 345-346: It is not well-described how the inverse radiative transfer model is used. What is the**
824 **forward RT model?**

825 Thanks to the reviewer for the question. The simulations are based on a plane-parallel approximation (see *Ulaby,*
826 *2014*) and the gas absorption model is described by *Rosenkrantz, 1998*. The text has been modified (see answer to
827 Comment 1.15).

828

829 The text has been modified

830 from:

831 *The RMSE between simulated clear-sky TBs - based on the mean emissivity values estimated for each class - and*
832 *the coincident observed clear-sky TBs appears to be too high to implement a robust signal analysis (>10 K).*

833 to:

834 *The clear-sky radiative transfer model simulations are based on the mean emissivity values estimated for each*
835 *class, and simulated by using the plane-parallel approximation (Ulaby & Long, 2014) and the Rosenkrantz gas*
836 *absorption model (Rosenkrantz, 1998) - The RMSE between simulated clear-sky TBs and the coincident observed*
837 *clear-sky TBs appears to be too high to implement a robust signal analysis (>10 K).*

838

839 The following reference has been added to the text (Line 756):

840 *Rosenkrantz, P. W., Water vapor microwave continuum absorption: A comparison of measurements and models.*
841 *Radio Science, 33(4), 919-928. <https://doi.org/10.1029/98RS01182>, 1998.*

842

843 References:

844 Rosenkrantz, P. W., Water vapor microwave continuum absorption: A comparison of measurements and models.
845 *Radio Science, 33(4), 919-928. <https://doi.org/10.1029/98RS01182>, 1998.*

846

847 Ulaby, F., & Long, D., Microwave radar and radiometric remote sensing, 1st Edition, the Univ. of Michigan Press,
848 ISBN: 978-0-472-11935-6, 2014.

849

850 **2.11) Lines 362-365: How emissivity is used for calculating the simulated TBs? It seems recursive to use the**
851 **observations to estimate the emissivity and then use it for retrievals. Please clarify whether the used**
852 **emissivities are dynamic or static.**

853 Thanks to the reviewer for the comment. The emissivity values are retrieved for each pixel and are used to estimate
854 the simulated TBs. Only low-frequency channels are used to classify the observations (by using PESCA) and to
855 retrieve an emissivity spectrum for the observations. Then, this spectrum has been used to estimate the TBs for
856 all ATMS channels. So the process is not recursive. The emissivities are used dynamically because they have been
857 calculated for each observation (see answer to Comment 2.2).

858 **2.12) Table 3: The parameters mentioned in the table are different than the ones mentioned in the text in**
859 **lines 435-437.**

860 Thanks to the reviewer for the comment. The Table has been changed:

861

862

863

864

865

866 from:

867

Predictor Set	POD	FAR	HSS
$\Delta TB_{obs-sim}$	0.75	0.29	0.48
TB_{obs}	0.81	0.18	0.65
$TB_{obs}+environmental\ var$	0.82	0.17	0.68
$TB_{obs}+\Delta TB_{obs-sim}$	0.84	0.16	0.69

868 **Table 3: HANDEL-ATMS SSR Detection Performance: Statistical scores for different Predictor Sets**

869 to:

870

Predictor Set	POD	FAR	HSS
$\Delta TB_{obs-sim}+ ancillary\ parameters$	0.75	0.29	0.48
$TB_{obs}+ ancillary\ parameters$	0.81	0.18	0.65
$TB_{obs}+environmental\ variables+ ancillary\ parameters$	0.82	0.17	0.68
$TB_{obs}+\Delta TB_{obs-sim}+ ancillary\ parameters$	0.84	0.16	0.69

871 **Table 3: HANDEL-ATMS SSR Detection Performance: Statistical scores for different Predictor Sets**

872 Minor comments:

873 **2.13) Line 273: It is better to mention all the variables that have been used for training the network here.**

874 Thanks to the reviewer for the suggestion. The text has been changed

875 from:

876 *Four ANNs are then applied to a predictor set consisting of ATMS TB_{obs} , $\Delta TB_{obs-sim}$, a surface classification*

877 *flag, and other environmental and ancillary parameters.*

878 to:

879 *Four ANNs are then applied to a predictor set consisting of ATMS TB_{obs} , $\Delta TB_{obs-sim}$, a surface classification*

880 *flag, and other ancillary parameters (elevation and ATMS viewing angle for the final version).*

881

882 **2.14) line 203-204: list of environmental and ancillary parameters is not presented in the dataset.**

883 Thanks to the reviewer for the comment. The text has been changed

884 from:

885 *Some model-derived variables have been added to the dataset to be used as ancillary variables.*

886

887

888

889 to:
890 *Some model-derived variables, specifically Total Precipitable Water (TPW), the 2-m Temperature (T_{2m}), the Skin*
891 *Temperature, the freezing level height and the temperature and humidity profiles, have been added to the dataset*
892 *to be used as ancillary parameters.*

893

894 **2.15) Line 356: "...for ocean and land respectively."**

895 Thanks to the reviewer for the correction.

896 The text has been changed

897 from:

898 *The estimated spectra are shown in Figure 4 and Figure 5 for the land and ocean classes, respectively.*

899 to:

900 *The estimated spectra are shown in Figure 4 and Figure 5 for ocean and land respectively.*

901

902

903 **2.16) Line 387: What is the used atmospheric radiative transfer model? Please spell out RTM.**

904 Thanks to the reviewer for the comment. The model used is that described by *Rosenkranz, 1998*. The text has been
905 modified

906 from:

907 *An emissivity spectrum, (calculated as the mean of the emissivity values for each cluster), together with ECMWF*
908 *temperature and water vapor profiles, is used as input in the RTM to simulate the clear-sky TBs.*

909 to

910 *An emissivity spectrum, (calculated as the mean of the emissivity values for each cluster), together with ECMWF*
911 *temperature and water vapor profiles, is used as input in the radiative transfer model (RTM) (see *Ulaby & Long**
912 *,2014, *Rosenkranz, 1998*) to simulate the clear-sky TBs.*

913

914 References:

915 Rosenkranz, P. W., Water vapor microwave continuum absorption: A comparison of measurements and models.
916 *Radio Science*, 33(4), 919-928. <https://doi.org/10.1029/98RS01182>, 1998.

917

918 Ulaby, F., & Long, D., Microwave radar and radiometric remote sensing, 1st Edition, the Univ. of Michigan Press,
919 ISBN: 978-0-472-11935-6, 2014.

920 **2.17) Table 2: What is the accuracy represented here? The accuracy of PESCA for surface classification?**

921 Thanks to the reviewer for the comment. The accuracy represented here is the ratio between the number of
922 observations where both SOM and LDA identify the same cluster and the total observations of the class.

923

924 **2.18) Line 489: Remove the dot at the beginning of the sentence.**

925 Thanks to the reviewer for the correction. The text has been largely modified to address some comments by
926 Reviewer 1.

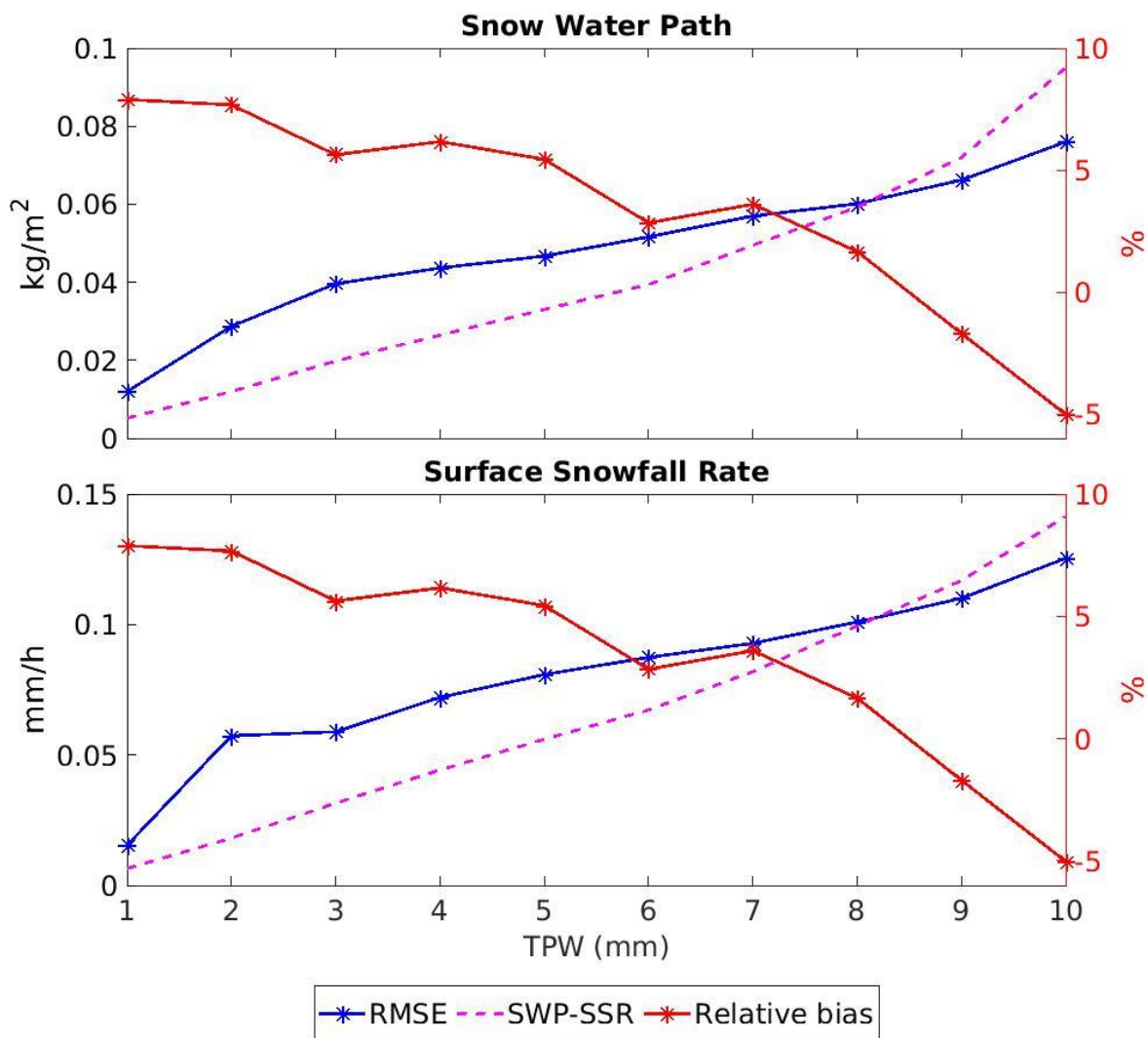
927 from:

928 . Generally, it can be observed that, although HANDEL-ATMS is able to detect extremely light snowfall events, it
929 does not have the sensitivity to correctly estimate their intensity.

930 to:

931

932 Figure 11 shows the dependence of HANDEL-ATMS snowfall estimation error statistics, as well of SWP and SSR,
933 on TPW . The curves represent the mean SWP or SSR computed for each 1-mm TPW bin, the RMSE and the
934 relative bias (the ratio between the bias and the SWP/SSR mean value for each bin). TPW and snowfall intensity
935 are strongly correlated. An increase of the absolute RMSE can be observed as TPW increases, and it is larger
936 than the SWP/SSR mean value for TPW < 8 mm. A similar behavior can be observed by analyzing the dependence
937 of HANDEL-ATMS snowfall estimation error statistics on T_{2m} (not shown). A very moderate overestimation is
938 observed for TPW < 8 mm and for lower SWP and SSR values (< 0.1 mm/h), with relative bias around 5%, (up
939 to 8% only for extremely low TPW values and very low number of observations (see Figure 7)), while
940 underestimation (relative bias up to -5%) is observed for higher TPW values and higher SWP and SSR values.
941 So, it can be concluded that HANDEL-ATMS has good detection capabilities (also for extremely light snowfall)
942 but it shows some limitations in correctly estimating its intensity, with slight overestimation of the very light
943 snowfall typical of high latitudes.



944
945

946 *Figure 11: HANDEL-ATMS SWP and SSR Detection Performances for different bins of TPW. The left y-axis*
947 *reports RMSE absolute values and the mean intensity value for each 1-mm TPW bin, while the relative bias,*
948 *calculated as the ratio between the bias and the SWP/SSR mean value for each bin.*

949

950 **2.19) Figure 1: The inputs of PESCA mentioned in this figure are not aligned with the original paper. For**
951 **example, there exists no explanation for the low-frequency ratio and scattering coefficients.**

952 Thanks to the reviewer for the comment. Indeed, there is not a direct mention of the PESCA input parameters;
953 however, these parameters are derived from the inputs cited in the box (low-frequency ratio is a ratio between two
954 $T_{B_{obs}}$, the scattering index is a difference between two $T_{B_{obs}}$, pem_{LF} is a ratio between a $T_{B_{obs}}$ and T_{2m} , see
955 *Camplani et al, 2021*). We wanted to highlight that we use the same inputs in more than one module - e. g., T_{Bs}
956 are used both for surface classification and snowfall detection and estimate. The same definition of the input
957 variables of PESCA can be found in the paper in section 3.1.1.

958 References:

959

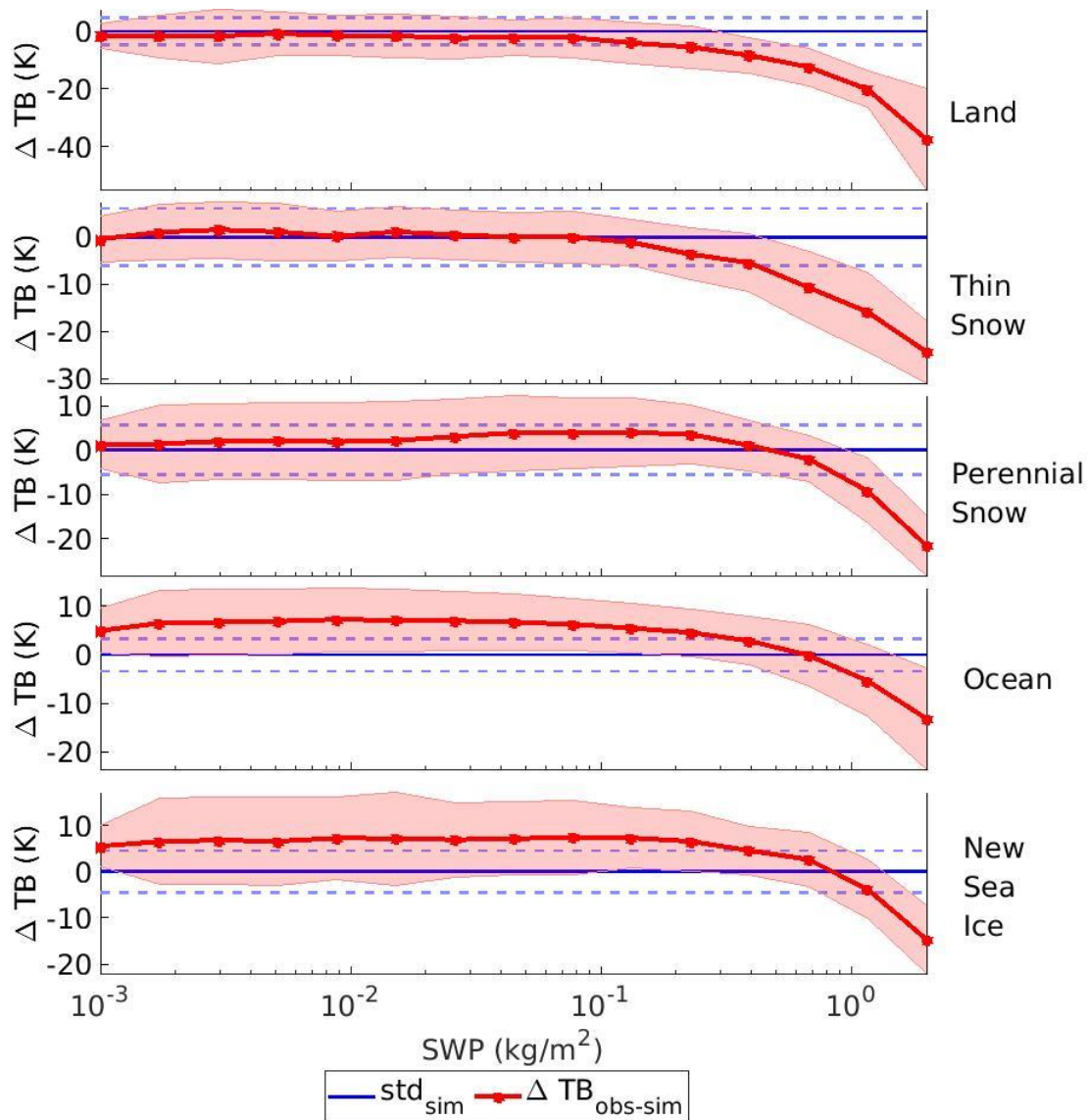
960 Camplani, A., Casella, D., Sanò, P., & Panegrossi, G.: The Passive microwave Empirical cold Surface
961 Classification Algorithm (PESCA): Application to GMI and ATMS. *Journal of Hydrometeorology*, 22(7), 1727-
962 1744, <https://doi.org/10.1175/JHM-D-20-0260.1>, 2021.

963 **2.20) Figure 6: No results are presented over sea ice.**

964 Thanks to the reviewer for the comment.

965 Figure 6 has been modified, with two new subplots related to two PESCA classes (Ocean and New sea Ice).

966



967
 968
 969
 970
 971
 972
 973
 974
 975
 976
 977
 978
 979
 980
 981
 982
 983
 984
 985
 986
 987

The following statement has been added to the text (line 423):

For what concerns ocean and new sea ice classes, a clear scattering signal is visible only for high SWP values (> 1 kg m⁻²) while for low SWP values a significant emission signal is observed. The ubiquitous presence of supercooled water layers in snowing clouds (Wang et al, 2013, Battaglia & Panegrossi 2020), especially over oceans (Battaglia & Delanoë, 2013), generates an emission effect which is particularly significant over radiatively cold surfaces (such as Ocean and New Sea Ice at high frequency, see Figure 4), and can mask or overcome the weak scattering signal generated by falling snow especially in light snowfall events. It is also important to underline that the DARDAR product identifies only supercooled water layers at the cloud top (Panegrossi et al., 2017), while it has been shown that the impact of supercooled water layers embedded in the clouds can be very significant on the measured TBs at MW high frequency window channels (Battaglia & Panegrossi, 2020, Panegrossi et al., 2022). It is very likely that the emission effect observed over ocean and sea ice is generated by supercooled liquid layers which are not identified by the DARDAR product.

Figure 6 caption has been modified accordingly from:

Figure 6: 165.5 GHz Snowfall Signature as a function of SWP for three Land surface Classes. The red line and shaded areas represent the mean values and standard deviations of $\Delta TB_{obs-sim}$ (i.e., the snowfall signature) while the blue lines are centered on the estimated bias and standard deviation of $\Delta TB_{obs-sim}$ in clear sky conditions for the corresponding PESCA surface class.

988 to:

989 *Figure 6: 165.5 GHz Snowfall Signature as a function of SWP for five PESCA surface classes. The red line and*
990 *shaded areas represent the mean values and standard deviations of $\Delta TB_{obs-sim}$ (i.e., the snowfall signature)*
991 *while the blue lines are centered on the estimated bias and standard deviation of $\Delta TB_{obs-sim}$ in clear sky*
992 *conditions for the corresponding PESCA surface class.*

993

994 The following reference has been added to the text (Line 798):

995

996 Wang, Y., Liu, G., Seo, E. K., & Fu, Y.: *Liquid water in snowing clouds: Implications for satellite remote sensing*
997 *of snowfall. Atmospheric research, 131, 60-72, <https://doi.org/10.1016/j.atmosres.2012.06.008>, 2013.*

998

999 References:

1000

1001 Battaglia, A., & Delanoë, J.: Synergies and complementarities of CloudSat-CALIPSO snow observations. *Journal*
1002 *of Geophysical Research: Atmospheres, 118(2), 721-731. <https://doi.org/10.1029/2012JD018092>, 2013.*

1003

1004 Battaglia, A., & Panegrossi, G.: What can we learn from the CloudSat radiometric mode observations of snowfall
1005 over the ice-free ocean?. *Remote Sensing, 12(20), 3285, <https://doi.org/10.3390/rs12203285>, 2020.*

1006

1007 Panegrossi, G., Rysman, J. F., Casella, D., Marra, A. C., Sanò, P., & Kulie, M. S.: CloudSat-based assessment of
1008 GPM Microwave Imager snowfall observation capabilities. *Remote Sensing, 9(12), 1263,*
1009 *<https://doi.org/10.3390/rs9121263>, 2017.*

1010

1011 Panegrossi, G., Casella, D., Sanò, P., Camplani, A., & Battaglia, A.: Recent advances and challenges in satellite-
1012 based snowfall detection and estimation. *Precipitation Science, 333-376, [https://doi.org/10.1016/B978-0-12-](https://doi.org/10.1016/B978-0-12-822973-6.00015-9)*
1013 *[822973-6.00015-9](https://doi.org/10.1016/B978-0-12-822973-6.00015-9), 2022.*

1014

1015 Wang, Y., Liu, G., Seo, E. K., & Fu, Y.: *Liquid water in snowing clouds: Implications for satellite remote sensing*
1016 *of snowfall. Atmospheric research, 131, 60-72, <https://doi.org/10.1016/j.atmosres.2012.06.008>, 2013.*

1017

1018

1019

1020 **2.21) Figure 10: Please mention that the shown green dots denote the CPR overpass.**

1021 Thanks to the reviewer for the suggestion. The caption of Figures 10 12, and 13 (now Figures 12, 14, and 15) has
1022 been changed

1023 Figure 10/12:

1024 from:

1025 *Figure 10: Greenland - 2016/04/24 - PESCA Background Surface Classification.*

1026 to:

1027 *Figure 12: Greenland - 2016/04/24 - PESCA Background Surface Classification. The green dotted line*
1028 *represents the CloudSat track.*

1029

1030

1031

1032

1033 Figure 12/14:

1034 from:

1035 *Figure 12: Greenland - 2016/04/24 - 165 GHz Channel measured TB ($T_{B_{obs}}$) (top panel) and the deviation of*
1036 *$T_{B_{obs}}$ from the simulated clear-sky TBs ($\Delta T_{B_{obs-sim}}$) (bottom panel)*

1037

1038 to:

1039 *Figure 14: Greenland - 2016/04/24 - 165 GHz Channel measured TB ($T_{B_{obs}}$) (top panel) and the deviation of*
1040 *$T_{B_{obs}}$ from the simulated clear-sky TBs ($\Delta T_{B_{obs-sim}}$) (bottom panel). The red dotted line (top*
1041 *panel) and the green dotted line (bottom panel) represent the CloudSat track.*

1042 Figure 13/15:

1043 from:

1044 *Figure 13: Greenland - 2016/04/24 - Maps of the HANDEL-ATMS module's output: the SWP detection mask*
1045 *(top panel), the estimated SWP (kg m^{-2}) (second panel), the SSR detection mask (third panel), the estimated SSR*
1046 *(mm h^{-1}) (bottom panel).*

1047

1048

1049 to:

1050 *Figure 15: Greenland - 2016/04/24 - Maps of the HANDEL-ATMS module's output: the SWP detection mask*
1051 *(top panel), the estimated SWP (kg m^{-2}) (second panel), the SSR detection mask (third panel), the estimated SSR*
1052 *(mm h^{-1}) (bottom panel). The green dotted lines (bottom panel) represent the CloudSat track.*

1053

1054